J|A|C|S
ARTICLES

Published on Web 03/11/2010

Facile Activation of Dihydrogen by a Phosphinito-Bridged Pt(I)−Pt(I) Complex

Piero Mastrorilli,*[,†] Mario Latronico,[†] Vito Gallo,[†] Flavia Polini,[†] Nazzareno Re,[‡] Alessandro Marrone,[‡] Roberto Gobetto,[§] and Silvano Ellena[§]

Dipartimento di Ingegneria delle Acque e di Chimica del Politecnico di Bari, Via Orabona 4, I-70125 Bari, Italy, Dipartimento di Scienze del Farmaco, Università "G. d'Annunzio", Via dei Vestini 31, 66100 Chieti, Italy, and Dipartimento di Chimica I.F.M., Università di Torino, Via P. Giuria 7, 10125 Torino, Italy

Received November 17, 2009; E-mail: p.mastrorilli@poliba.it

Abstract: The phosphinito-bridged Pt(I) complex [(PHCy$_2$)Pt(μ-PCy$_2$){κ^2*P,O*-μ-P(O)Cy$_2$}Pt(PHCy$_2$)](*Pt*−*Pt*) (**1**) reversibly adds H_2 under ambient conditions, giving *cis*-[(H)(PHCy$_2$)Pt^1(μ-PCy$_2$)(μ-H)Pt^2(PHCy$_2$){κ*P*-P(O)Cy$_2$}](*Pt*−*Pt*) (**2**). Complex **2** slowly isomerizes spontaneously into the corresponding more stable isomer *trans*-[(PHCy$_2$)(H)Pt(μ-PCy$_2$)(μ-H)Pt(PHCy$_2$){κ*P*-P(O)Cy$_2$}](*Pt*−*Pt*) (**3**). DFT calculations indicate that the reaction of **1** with H_2 occurs through an initial heterolytic splitting of the H_2 molecule assisted by the phosphinito oxygen with breaking of the Pt−O bond and hydrogenation of the Pt and O atoms, leading to the formation of the intermediate [(PHCy$_2$)(H)Pt(μ-PCy$_2$)Pt(PHCy$_2$){κ*P*-P(OH)Cy$_2$}](*Pt*−*Pt*) (**D**), where the two split hydrogen atoms interact within a six-membered Pt−H···H−O−P−Pt ring. Compound **D** is a labile intermediate which easily evolves into the final dihydride complex **2** through a facile (9−15 kcal mol^{-1}, depending on the solvent) hydrogen shift from the phosphinito oxygen to the Pt−Pt bond. Information obtained by addition of para-H_2 on **1** are in agreement with the presence of a heterolytic pathway in the **1** → **2** transformation. NMR experiments and DFT calculations also gave evidence for the nonclassical dihydrogen complex [(PHCy$_2$)(η^2-H$_2$)Pt(μ-PCy$_2$)Pt(PHCy$_2$){κ*P*-P(O)Cy$_2$}](*Pt*−*Pt*) (**4**), which is an intermediate in the dehydrogenation of **2** to **1** and is also involved in intramolecular and intermolecular exchange processes. Experimental and DFT studies showed that the isomerization **2** → **3** occurs via an intramolecular mechanism essentially consisting of the opening of the Pt−Pt bond and of the hydrogen bridge followed by the rotation of the coordination plane of the Pt center with the terminal hydride ligand.

Introduction

The activation of molecular hydrogen under mild conditions is a topic of paramount importance in catalysis,[1] hydrogen storage,[2] and biochemistry.[3] While for catalysis purposes the binding of H_2 to the complexes should be tight enough for allowing subsequent H transfer onto suitable organic (or inorganic) substrates, the application in hydrogen storage requires H_2 additions to be reversible.[4]

It is well-known that the activation of dihydrogen by transition-metal complexes proceeds through the formation of a σ adduct[5] which can evolve either into a dihydrido complex (deriving from oxidative addition of the bonded H_2, Scheme 1a) or into a monohydrido complex (stemming from deprotonation of the σ complex by a suitable base,[6] Scheme 1b). In this framework, the majority of the studies have dealt with mononuclear metal complexes, while relatively few examples involving polynuclear metal complexes have been described.[4,7]

Scheme 1. Activation of H_2 by Transition-Metal Complexes[a]

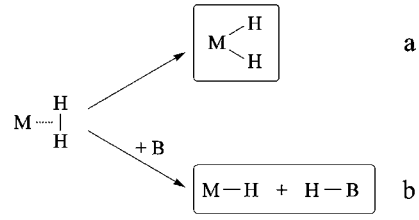

[a] B is a Lewis base which can be part of an internal ancillary ligand.

We have recently described the synthesis of the unsymmetrical phosphinito-bridged Pt(I) complex [(PHCy$_2$)Pt(μ-

[†] Politecnico di Bari.
[‡] Università "G. d'Annunzio".
[§] Università di Torino.

(1) (a) *Handbook of Homogeneous Hydrogenation*; de Vries, J. G., Elsevier, C. J., Eds.; Wiley-VCH: Weinheim, Germany, 2007. (b) Nishimura, S. *Handbook of Heterogeneous Catalytic Hydrogenation for Organic Synthesis*; Wiley: Chichester, U.K., 2001.
(2) (a) Yang, J.; Sudik, A.; Wolverton, C.; Siegel, D. J. *Chem. Soc. Rev.* **2010**, *39*, 656. (b) Kubas, G. J. *J. Organomet. Chem.* **2009**, *694*, 2648. (c) van den Berg, A. W. C.; Otero Areán, C. *Chem. Commun.* **2008**, 668. (d) Dincã, M.; Long, J. R. *Angew. Chem., Int. Ed.* **2008**, *47*, 6766. (e) Orimo, S.; Nakamori, Y.; Eliseo, J. R.; Zuttel, A.; Jensen, C. M. *Chem. Rev.* **2007**, *107*, 4111.
(3) Heinekey, D. M. *J. Organomet. Chem.* **2009**, *694*, 2671, and references therein.
(4) Weller, A. S.; McIndoe, J. S. *Eur. J. Inorg. Chem.* **2007**, 4411.
(5) (a) Kubas, G. J. *Proc. Natl. Acad. Sci. U.S.A.* **2007**, *104*, 6901. (b) Heinekey, D. M.; Oldham, W. J., Jr. *Chem. Rev.* **1993**, *93*, 913. (c) Crabtree, R. H. *Angew. Chem., Int. Ed. Engl.* **1993**, *32*, 789.
(6) Crabtree, R. H.; *The Organometallic Chemistry of the Transition Metals*, 4th ed.; Wiley-Interscience: Hoboken, NJ, 2005.
(7) Adams, R. D.; Captain, B. *Acc. Chem. Res.* **2009**, *41*, 409.

 10.1021/ja909747r

Scheme 2. Reaction Course for the Hydrogenation of **1**

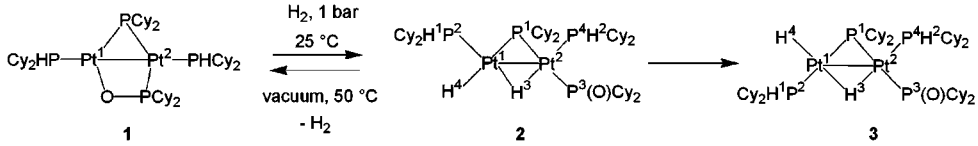

PCy_2){κ^2*P*,*O*-μ-P(O)Cy_2}Pt($PHCy_2$)] (*Pt*−*Pt*) (**1**),[8] which represents a potential candidate for H_2 activation under mild conditions, as it possesses an electrophilic center, the O-bound Pt atom,[9] capable of forming the σ adduct, as well as a potential base, the dicyclohexylphosphinite group, in close proximity to the hypothetical reactive center.

Here we describe the addition of dihydrogen to **1**, which proceeds in two steps: a facile and reversible uptake of H_2 to give the *cis*-dihydrido complex **2** and a consecutive irreversible slow isomerization into the corresponding *trans* isomer **3** (Scheme 2).

Addition of H_2 to 1

Bubbling H_2 under ambient conditions into a CH_2Cl_2 solution of **1** caused a complete conversion after 20 min of the starting material into *cis*-[(H)($PHCy_2$)Pt(μ-PCy_2)(μ-H)Pt($PHCy_2$){κ*P*-P(O)Cy_2}](*Pt*−*Pt*) (**2**), the first example of a diplatinum polyhydride species generated by direct addition of molecular hydrogen to a dinuclear complex.[10]

The structure of **2** was determined by multinuclear NMR spectroscopy. The $^{31}P\{^1H\}$ NMR spectrum in CH_2Cl_2 of **2** shows four signals, each flanked by ^{195}Pt satellites, centered at δ 119.2, 75.3, 11.3, and 9.5, respectively (Figure S1). Of these, the signal at δ 119.2 is attributable to the bridging phosphanide subtending a Pt−Pt bond (P^1), having in *trans* positions the phosphinito ligand ($^2J_{P(1),P(3)}$ = 245 Hz) and the terminal hydrido ligand ($^2J_{P(1),H(4)}$ =122 Hz, from the ^{31}P NMR spectrum, Figure S2). The signal at δ 75.3 is ascribed to the κ*P*-dicyclohexylphosphinito ligand, whereas the remaining two signals are attributable to the coordinated dicyclohexylphosphanes in *cis* positions with respect to the bridging phosphanide. In the ^{1}H NMR spectrum in CD_2Cl_2 (Figure S3), the bridging hydride shows a multiplet centered at δ −4.19 flanked by three sets of ^{195}Pt satellites from which the coupling constant values of $^1J_{H(3),Pt(1)}$ = 544 Hz and $^1J_{H(3),Pt(2)}$ = 591 Hz could be extracted, while the terminal hydride (δ −1.42), strongly coupled only with $^{195}Pt^1$ ($^1J_{H(4),Pt(1)}$ = 952 Hz), gives a doublet of doublets due to the couplings with the *trans*-P^1 ($^2J_{H(4),P(1)}$ = 118 Hz) and with the *cis*-P^2 ($^2J_{H(4),P(2)}$ = 27 Hz). In the $^1H\{^{31}P\}$ NMR spectrum, H^3 and H^4 appear as singlets (Figure 1), indicating that H−P scalar couplings are responsible for the multiplicity of the hydride signals in the ^{1}H NMR spectrum. The ^{195}Pt NMR signals (Figures S4 and S5) were found at δ −5901 (Pt^1) and δ −5584 (Pt^2) and are in line with those found for other systems having the $Pt_2(\mu\text{-H})(\mu\text{-}PR_2)$ core.[11] In the IR spectrum (KBr) the terminal and bridging hydrides gave stretching bands at 1935 cm^{-1} (medium) and 1636 cm^{-1} (weak), respectively.

The rate of hydrogenation for reactions in solution was found to be strongly dependent on the solvent. In fact, when the hydrogenation of **1** was carried out in aromatic solvents (toluene, benzene-d_6), the complete disappearance of **1** was achieved within 6 h, a time at which the reaction mixture was comprised of **2** and **3** in an approximately 2:1 ratio. A faster and more selective reaction occurred when ethanol was present in the reaction medium. Notably, the rate of H_2 uptake by **1** paralleled the amount of ethanol present in the mixture with the aromatic solvent, reaching a maximum (5 min necessary to convert completely **1** into **2**) for reactions carried out in pure ethanol (in this case the initial mixture was heterogeneous, due to the scarce solubility of **1** in ethanol).

Complex **2** was found to spontaneously isomerize into the more stable form *trans*-[($PHCy_2$)(H)Pt(μ-PCy_2)(μ-H)Pt($PHCy_2$)-{κ*P*-P(O)Cy_2}](*Pt*−*Pt*) (**3**) (Scheme 2), whose structure was unambiguously assigned on the basis of HR ESI-MS and multinuclear NMR data (Figures S8−S11). The **2** → **3** isomerization occurred both in solution and in the solid state. In dichloromethane the complete isomerization took 3 days at room temperature, and while it was stored in the solid state (under an N_2 atmosphere) **2** transformed after 6 days into a mixture containing 90% of **3** and 10% of **2**.

The formation of **2** is reversible: putting solid **2** under high vacuum at 323 K gave, after 3 h, the starting material **1** in 80% yield, the remainder being the *trans*-dihydride **3**.[12] Platinum-based compounds able to reversibly bind dihydrogen are $[Pt_2H(\mu\text{-dppm})_2]PF_6$,[13] $[Pt_2H(CO)(\mu\text{-dppm})_2]PF_6$(*Pt*−*Pt*),[14] $[Pt_4(PBu^t_3)_3\{PBu^t_2(CMe_2CH_2)\}]^+$,[15] platinum−gold clusters such as $[Pt(AuPPh_3)_8]^+$,[16] and clusters containing $Pt(PBu^t_3)$ groups.[7]

Differently from **2**, complex **3** was stable to dehydrogenation when put under vacuum at 323 K even after 6 days. Moreover,

(8) Gallo, V.; Latronico, M.; Mastrorilli, P.; Nobile, C. F.; Suranna, G. P.; Ciccarella, G.; Englert, U. *Eur. J. Inorg. Chem.* **2005**, 4607.

(9) Gallo, V.; Latronico, M.; Mastrorilli, P.; Polini, F.; Re, N.; Englert, U. *Inorg. Chem.* **2008**, *47*, 4785.

(10) Diplatinum polyhydrides were obtained by reaction of the following mononuclear complexes with molecular hydrogen. (a) $[Pt(C_2H_4)_2(PCy_3)]$: Green, M.; Howard, J. A. K.; Proud, J.; Spencer, J. L.; Stone, F. G. A.; Tsipis, C. A. *J. Chem. Soc., Chem. Commun* **1976**, 671. (b) $[Pt(C_2O_4)(PEt_3)_2]$: Paonessa, R. S.; Trogler, W. C. *Inorg. Chem.* **1983**, *22*, 1038. (c) $[\{(C_2F_5)PCH_2CH_2P(C_2F_5)_2\}PtMe(O_2CCF_3)]$: Bennet, B. L.; Roddick, D. M. *Inorg. Chem.* **1996**, *35*, 4703. Polyhydrido diplatinum complexes are also described in: (d) Leoni, P.; Manetti, S.; Pasquali, M. *Inorg. Chem.* **1995**, *34*, 749, and references therein. (e) Schwartz, D. J.; Andersen, R. A. *J. Am. Chem. Soc.* **1995**, *117*, 4014. (f) Albinati, A.; Bracher, G.; Carmona, D.; Jans, J. H. P.; Klooster, W. T.; Koetzle, T. F.; Macchioni, A.; Ricci, J. S.; Thouvenot, R.; Venanzi, L. M. *Inorg. Chim. Acta* **1997**, *265*, 255. (g) Mastrorilli, P.; Palma, M.; Fanizzi, F. P.; Nobile, C. F. *Dalton Trans.* **2000**, 4272. (h) Mastrorilli, P.; Nobile, C. F.; Fanizzi, F. P.; Latronico, M.; Hu, C.; Englert, U. *Eur. J. Inorg. Chem.* **2002**, 1210. (i) Bandini, A. L.; Banditelli, G.; Manassero, M.; Albinati, A.; Colognesi, D.; Eckert, J. *Eur. J. Inorg. Chem.* **2003**, 3958. (j) Itazaki, M.; Nishihara, Y.; Osakada, K. *Organometallics* **2004**, *23*, 1610. (k) Novio, F; Gonzáles-Duarte, P; Lledós; Mas-Ballesté, R *Chem. Eur. J.* **2007**, *13*, 1047.

(11) Mastrorilli, P. *Eur. J. Inorg. Chem.* **2008**, 4835.

(12) The dehydrogenation of **2** to give **1** occurred also at room temperature but was significantly slower. For example, after 4 days a mixture consisting of **3** (50%), **2** (35%), and **1** (15%) was obtained.

(13) (a) Foley, H. C.; Morris, R. H.; Targos, T. S.; Geoffroy, G. L. *J. Am. Chem. Soc.* **1981**, *103*, 7337. (b) Hill, R. H.; De Mayo, P.; Puddephatt, R. J. *Inorg. Chem.* **1982**, *21*, 3642.

(14) Fisher, J. R.; Mills, A. J.; Sumner, S.; Brown, M. P.; Thomson, M. A.; Puddephatt, R. J.; Frew, A. A.; Manojlovic-Muir, L.; Muir, K. W. *Organometallics* **1982**, *1*, 1421.

(15) Goodfellow, R. J.; Hamon, E. M.; Howard, J. A. K.; Spencer, J. L.; Turner, D. G. *J. Chem. Soc., Chem. Commun.* **1984**, 1604.

(16) (a) Aubart, M. A.; Pignolet, L. H. *J. Am. Chem. Soc.* **1992**, *114*, 7901. (b) Aubart, M. A.; Chandler, B. D.; Gould, R. A. T.; Krogstad, D. A.; Schoondergeng, M. F. J.; Pignolet, L. H. *Inorg. Chem.* **1994**, *33*, 3724.

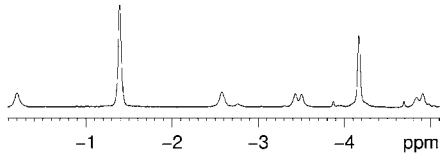

Figure 1. $^1H\{^{31}P\}$ NMR spectra of **2** (hydride region, 298 K, $CDCl_3$).

keeping a toluene solution of **3** at 363 K for 90 min resulted only in the onset of decomposition, but neither **1** nor **2** was formed.

It is worth noting that **2** (as well as **3**) was resistant to deprotonation when treated with a concentrated NaOH solution, in contrast to the related $[(X)(PHCy_2)Pt(\mu\text{-}PCy_2)(\mu\text{-}H)Pt(PHCy_2)\{\kappa P\text{-}P(O)Cy_2\}](Pt-Pt)$ compounds (X = Cl, Br), which were smoothly transformed into **1**. In fact, while quantitative transformation of $[(X)(PHCy_2)Pt(\mu\text{-}PCy_2)(\mu\text{-}H)Pt(PHCy_2)\{\kappa P\text{-}P(O)Cy_2\}](Pt-Pt)$ into **1** was observed after 24 h (X = Cl) or 48 h (X = Br) reaction,[17] no appreciable reaction occurred after 3 days when **2** was reacted with NaOH(conc). Since no deprotonation was observed for the *cis*-$[(X)(PHCy_2)Pt(\mu\text{-}PCy_2)(\mu\text{-}H)Pt(PHCy_2)\{\kappa P\text{-}P(O)Cy_2\}](Pt-Pt)$ compound when X = I,[18] it may be argued that the ability of the X ligand as a leaving group plays a role in the effectiveness of the deprotonation reaction.

Treating complexes **2** and **3** with an equimolar amount of HBF_4 (as the dimethyl ether adduct) resulted in the smooth protonation of the phosphinito oxygen to give the corresponding species *cis*- and *trans*-$[(PHCy_2)(H)Pt(\mu\text{-}PCy_2)(\mu\text{-}H)Pt(PHCy_2)\{\kappa P\text{-}P(OH)Cy_2\}]BF_4(Pt-Pt)$ as a result of the higher basicity, in our system,[17] of the PO ligand compared to that of the Pt or of the hydride centers.[19]

The addition of D_2 to **1** to give **2**-d_2 was slower than the addition of H_2 under the same conditions, and a kinetic isotope effect (KIE) of 1.4 was determined. This value is in line with those obtained for the addition of H_2 to $[Pt_3Re_2(CO)_6(PBu^t_3)_3]$ (KIE = 1.3)[20] or to $[Pt_2Re_2(CO)_7(PBu^t_3)_2(\mu\text{-}H)_2]$ (KIE = 1.5).[21]

Variable amounts of **2**-d_2 were detected by ^2H and ^{31}P NMR also when **2** was left in CH_2Cl_2 solution under a D_2 atmosphere. Interestingly, isotopic exchange occurred also in the solid state when solid **2** was left under sonication in a D_2 atmosphere at room temperature for 2 days. A plausible mechanism that explains such a behavior involves the intermediacy of the nonclassical dihydrogen complex $[(PHCy_2)(\eta^2\text{-}H_2)Pt(\mu\text{-}PCy_2)Pt(PHCy_2)\{\kappa P\text{-}P(O)Cy_2\}](Pt-Pt)$ (**4**), in equilibrium with **2**, capable of exchanging D_2 for H_2 (Scheme 3). Conversely, when **2**-d_2 was left in CD_2Cl_2 solution under a H_2 atmosphere, the appearance of the hydridic ^1H NMR signals of **2** was detected. The σ-bonded dihydrogen complex **4** might also be

Scheme 3. D_2/H_2 Exchange in **2**

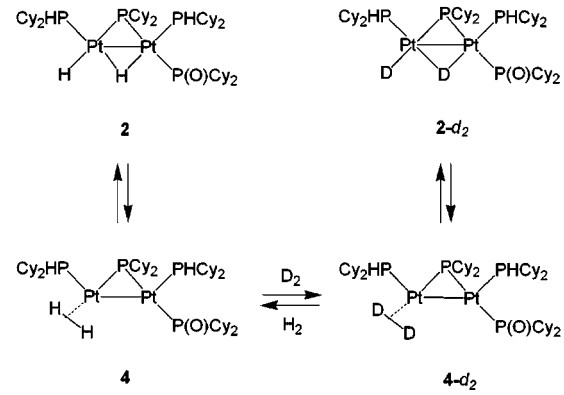

invoked as a possible intermediate in the transformation of **1** into **2** and vice versa.

The Nonclassical Dihydrogen Complex 4

In the literature, platinum complexes with σ-bonded dihydrogen are rare if compared, for instance, to d^6 metals[22] and consist only of the mononuclear Pt^{II} species *trans*-$[PtH(\eta^2\text{-}H_2)(PR_3)_2]^+$ (R = Bu^t,[23] Pr^i [24]) and *trans*-$[Pt(PCy_3)_2L(\eta^2\text{-}H_2)]^+$ (L = H, CH_3, Ph).[25] A Pt^0 η^2-dihydrogen complex was proposed to explain the dynamic process observed in solutions of $[\{Cy_2P(CH_2)_nPCy_2\}PtH_2]$ (n = 3, 4).[26]

We gained evidence by means of NOESY-EXSY experiments that the equilibrium between **2** and the nonclassical dihydrogen complex **4** does exist and that such an equilibrium is completely shifted toward **2**.

Figure 2 shows a portion of the $^1H\{^{31}P\}$NOESY-EXSY spectrum recorded for a CD_2Cl_2 solution of **2** at 298 K in which correlations indicating the chemical exchange between the terminal hydride (δ −1.4) and the bridging hydride (δ −4.2) are present.

Preliminarily, it is advisable to recall that the cross peaks between the signals of the mutually *cis* hydrides are the result of two contributions with opposite sign. In fact, the sign of the diagonal peaks being positive, a negative contribution comes from the dipolar coupling between the two hydride nuclei in close spatial proximity, and a positive contribution is generated by their chemical exchange. Thus, the sign of the cross peaks depends on the relative intensity of the exchange over the dipolar coupling contributions: a positive sign of the cross peak is the result of a dynamic process with an exchange frequency sufficiently high to override the dipolar coupling contribution, while a negative sign of the cross peak has to be expected when the dipolar coupling contribution prevails.

In the spectrum shown in Figure 2, the cross peak circled in yellow accounts for the chemical exchange between the terminal and the bridging hydrides in the isotopologue of **2** containing no ^{195}Pt atoms (yellow box) but does not give any indication of the exchange mode: i.e., whether it is inter- or intramolecular. On the other hand, the exchange mode was ascertained to be

(17) Latronico, M.; Polini, F.; Gallo, V.; Mastrorilli, P.; Calmuschi-Cula, B.; Englert, U.; Re, N.; Repo, T.; Raisanen, M. *Inorg. Chem.* **2008**, *47*, 9779.
(18) Latronico, M.; Gallo, V.; Mastrorilli, P. Unpublished results.
(19) Main NMR features of *cis*-$[(P^1HCy_2)(H^1)Pt(\mu\text{-}P^2Cy_2)(\mu\text{-}H^2)Pt(P^3HCy_2)\{\kappa P^4\text{-}P(OH^3)Cy_2\}]^+(Pt-Pt)$ (298 K, CD_2Cl_2): $\delta_{P(1)} \approx \delta_{P(3)}$ 11, $\delta_{P(2)}$ 132.1, $\delta_{P(4)}$ 96, $^1J_{P(2),P(4)}$ = 247 Hz; $\delta_{H(1)}$ −1.42, $\delta_{H(2)}$ −4.47, $\delta_{H(3)}$ 5.56. Main NMR features of *trans*-$[(H^1)(P^1HCy_2)Pt(\mu\text{-}P^2Cy_2)(\mu\text{-}H^3)Pt(P^3HCy_2)\{\kappa P^4\text{-}P(OH^3)Cy_2\}]^+(Pt-Pt)$ (298 K, CD_2Cl_2): $\delta_{P(1)}$ 11.8, $\delta_{P(2)}$ 152.0, $\delta_{P(3)}$ 0.0, $\delta_{P(4)}$ 126.1, $^1J_{P(2),P(4)}$ = 262 Hz, $^1J_{P(1),P(2)}$ = 271 Hz; $\delta_{H(1)}$ −5.39, $\delta_{H(2)}$ −6.25, $\delta_{H(3)}$ 6.3.
(20) Adams, R. D.; Captain, B.; Beddie, C.; Hall, M. B. *J. Am. Chem. Soc.* **2007**, *129*, 986.
(21) Adams, R. D.; Captain, B.; Smith, M. D.; Beddie, C.; Hall, M. B. *J. Am. Chem. Soc.* **2007**, *129*, 5981.
(22) Kubas, G. J. *Chem. Rev.* **2007**, *109*, 4152.
(23) Gusev, D. G.; Notheis, J. U.; Rambo, J. R.; Hauger, B. E.; Eisenstein, O.; Caulton, K. G. *J. Am. Chem. Soc.* **1994**, *116*, 7409.
(24) Butts, M. D.; Scott, B. L.; Kubas, G. J. *J. Am. Chem. Soc.* **1994**, *116*, 7409.
(25) Stahl, S. S.; Labinger, J. A.; Bercaw, J. E. *Inorg. Chem.* **1998**, *37*, 2422.
(26) Clark, H. C.; Hampden Smith, M. J. *J. Am. Chem. Soc.* **1986**, *108*, 3829.

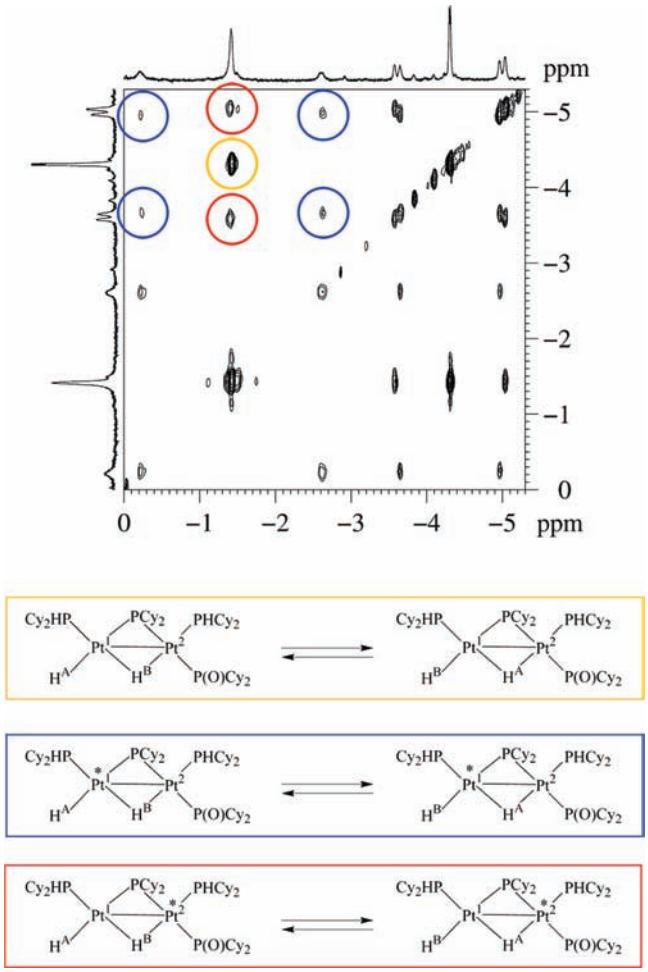

Figure 2. $^1H\{^{31}P\}$ EXSY spectrum of a CD_2Cl_2 solution of **2** (hydride region, $T = 298$ K). NMR-active Pt atoms are denoted with an asterisk.

intramolecular by the analysis of the cross peaks, circled in blue and red, generated by the isotopologues containing one ^{195}Pt atom.[27] The peaks circled in blue indicate that the terminal hydride H^A is scalar coupled to the NMR-active Pt^1 and preserves the coupling when its chemical identity changes into the bridging hydride H^B (blue box). Moreover, the peaks circled in red are generated when the terminal hydride H^A, initially bound to a non-NMR-active Pt atom, passes to the bridging position, in which it couples with the NMR-active Pt^2 (red box).

These findings strongly confirm the intermediacy of the σ adduct **4** in the dynamic process and can be explained by admitting that the rotation of the dihydrogen molecule, *which remains coordinated to the metal center* in **4**, is responsible for the hydride exchange (Scheme 4).[28] The alternative intermolecular path consisting of the possible decoordination and recoordination of dihydrogen would generate correlations between each central hydride signal and *all* of the satellite signals, giving a pattern different from that experimentally observed in Figure 2. However, since the observed H_2/D_2 exchange can be explained only in terms of intermolecular paths, it can be concluded that its contribution to the exchange is negligible.

The elusiveness of **4**, which was never directly detected by NMR analyses even at low temperature, and the lack of isotope shift on passing from **2** to the deuterated complex **2**-d_2[29] concur to indicate that only a very small amount of **4** is present in equilibrium with **2**. Moreover, the sharpness of the ^{195}Pt satellites for both ^1H NMR hydride signals indicates that the transformation **2** → **4** (and reverse) is slow on the NMR time scale. Accordingly, a significant difference was found in the T_1 values for the bridging hydride ($T_1 = 411$ ms) and the terminal hydride ($T_1 = 462$ ms).[30]

We addressed also the possibility that complex **4** might be the precursor of **2** during the hydrogenation of **1**. First of all, we tried to detect long-lived reaction intermediates by multinuclear 1D and 2D (^1H and ^{31}P EXSY) NMR experiments carried out in the first stages of the H_2 uptake in benzene-d_6 or in CD_2Cl_2 (in this case also at low T), but in all cases only signals attributable to **1** and **2** were observed. The absence of signals other than those of **1** and **2** indicates that, if involved in the hydrogenation of **1**, complex **4** had to represent a short-lived intermediate that, as soon as it forms, evolves toward **2**. This transformation conceivably occurs via a homolytic breaking of the H−H bond in the coordinated H_2, so that it should be possible to confirm by exploiting PHIP (para-hydrogen induced polarization) induced by the use of para-H_2.[31] However, when para-H_2 was reacted with **1** under several experimental conditions, no hyperpolarization was detected, indicating that the homolytic path leading from **4** to **2** is unlikely and that presumably **4** is not a precursor of **2**.

para-H_2 Study

A series of para-hydrogen experiments were performed in order to fully understand the mechanism of hydrogen addition on complex **1**.

It is well-known that PHIP effects can be observed only under the following conditions:[32]

- Spin correlation must be saved during the hydrogenation process; in other words, both para-hydrogen nuclei must be transferred into the same product during the reaction, keeping their spin−spin coupling.
- The symmetry of the para-hydrogen molecule must be broken at the same stage during the reaction.
- The relaxation rate of the para-hydrogenated intermediates or products must be relatively slow.

Several different items can be in principle obtained by para-hydrogen experiments, but the presence or the absence of hyperpolarized signals represents a valuable method to discriminate between different reaction pathways. A large number of transient species and reaction pathways detected by para-hydrogen experiments is now available in the literature.[33]

(27) The hydride exchange in the isotopologue containing both $^{195}Pt^1$ *and* $^{195}Pt^2$ is too weak to be detected.

(28) The same consideration holds for the experiment carried out in the less polar C_6D_6. In this case, the cross-peak sign was found to be temperature-dependent, being negative at 298 K and positive at 353 K. This behavior can be explained by admitting that at room temperature the exchange contribution is less than the dipolar coupling contribution, due to a low H^3-H^4 exchange rate, and that on increasing the T, the exchange frequency becomes sufficiently high to give a net positive peak.

(29) Bergamo, M.; Beringhelli, T.; D'Alfonso, G.; Mercandelli, P.; Sironi, A. *J. Am. Chem. Soc.* **2002**, *124*, 5117.

(30) A fast equilibrium between **2** and **4** would result in an averaged T_1 for the different types of hydrides.

(31) PHIP leads to enhanced absorption and emission resonances in product NMR spectra when a reaction is done with hydrogen enriched in the para spin state, and the addition of hydrogen occurs such that spin correlation of the transferred protons is maintained throughout the reaction: Millar, S. P.; Jang, M.; Lachicotte, R. J.; Eisenberg, R. *Inorg. Chim. Acta* **1998**, *270*, 363.

(32) Natterer, J.; Bargon, J. *Prog. Nucl. Magn. Reson. Spectrosc.* **1997**, *31*, 293.

Scheme 4. Intramolecular Exchange between Terminal and Bridging Hydrides of **2**

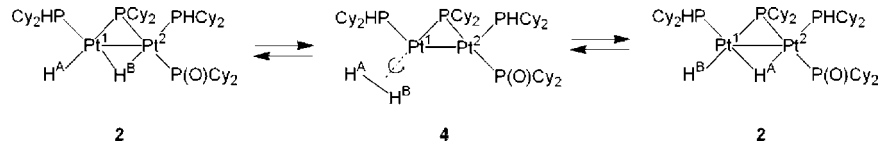

2 **4** **2**

Scheme 5. Possible Mechanisms for the **2** → **3** Isomerization

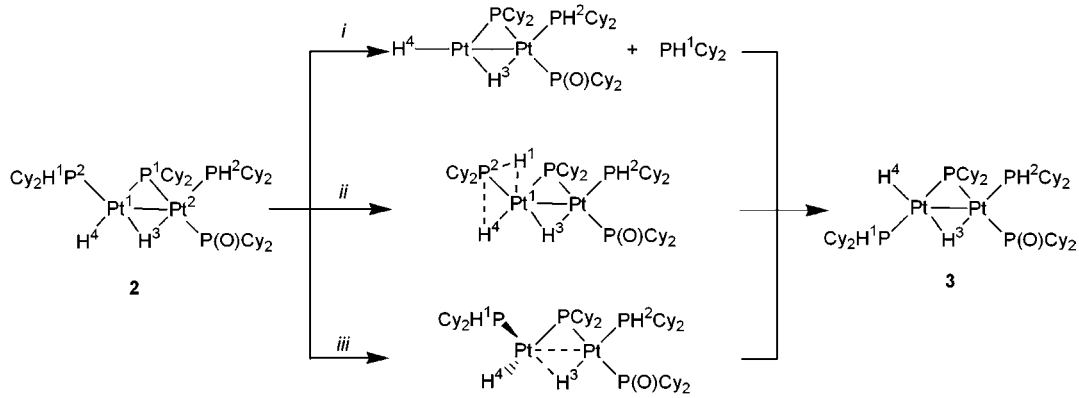

We performed a series of para-hydrogen ALTADENA (adiabatic longitudinal transport and dissociation engenders net alignment) experiments[34] on **1** in benzene-d_6 solution at different temperatures in the range 298−323 K, but no polarized signals were observed. The same reaction was repeated by using as solvent benzene-d_6 containing a catalytic quantity of ethanol-d_6 (5 μL), CD_2Cl_2, or pure ethanol-d_6, but in all cases no hyperpolarized peaks were detected. Also by performing a PASADENA (para-hydrogen and synthesis allows dramatically enchanced signal alignment) experiment[35] on **1** we observed only an efficient **1** → **2** conversion without the presence of hyperpolarized signals.

Two alternative hypotheses can be proposed for explaining all these results: (a) a low reaction rate and/or a high relaxation rate of the hyperpolarized species and (b) a heterolytic hydrogen cleavage. Hypothesis a can be ruled out, since the reaction rate is rather high and the relaxation times are in the range of 0.4−0.5 s (see above). Thus, the lack of hyperpolarized signals is likely due to the occurrence of a heterolytic hydrogen cleavage mechanism in the **1** → **2** transformation.

Isomerization from 2 to 3

With regard to the isomerization mechanism from **2** to **3**, at least three hypotheses can be put forward: (i) a dissociative pathway via tricoordinate Pt^1; (ii) an intramolecular rearrangement via activation and rupture of the P^2-H^1 bond; (iii) a direct intramolecular rearrangement via an out-of-plane slippage of the terminal hydride (Scheme 5).

In order to check the dissociative mechanism (path i) we carried out a ^{31}P NMR analysis of a solution of **2** in toluene-d_8, but neither was any trace of free $PHCy_2$ (δ_P −27) found in the $^{31}P\{^1H\}$ NMR spectrum nor were exchange cross peaks in the region of the coordinated P^2HCy_2 present in the $^{31}P\{^1H\}$ EXSY spectra recorded at various temperatures and various mixing times.[36] These findings suggest that path i has to be discarded, in agreement with the occurrence of the isomerization also in the solid state, where dissociative processes are not favored.[37]

The second hypothesis envisages the exchange between H^1 (the hydrogen originally bound to P^2) and the terminal hydride H^4, leading to the thermodynamically more stable **3**. Such an exchange might occur either via a transition state containing a hypervalent phosphorus (as shown in Scheme 5) or via the oxidative addition of the P^2-H^1 bond to Pt^1 followed by the formation of the P^2-H^4 bond. In any case, the isomerization of the deuterated compound **2**-d_2 should result in the formation of the complex *trans*-[(H)($PDCy_2$)Pt(μ-PCy_2)(μ-D)Pt($PHCy_2$){κP-$P(O)Cy_2$}], having the coordinated P^2DCy_2 and the unlabeled terminal hydride. Carrying out the isomerization of **2**-d_2 resulted exclusively in the dideuterido complex *trans*-[(D)($PHCy_2$)Pt(μ-PCy_2)(μ-D)Pt($PHCy_2$){κP-$P(O)Cy_2$}](*Pt*−*Pt*) (**3**-d_2), showing no "labeling" of the coordinated P^2HCy_2 and indicating that path ii is not operative.

The intramolecular rearrangement constituting path iii seems therefore favored, and it is consistent with the observed isomerization in the solid state. Such a mechanism is difficult to prove experimentally but was confirmed by DFT studies, as discussed below.

DFT Study

Density functional calculations were performed to investigate the possible mechanism for the reaction of **1** with H_2 (and the reverse) and for the subsequent **2** → **3** isomerization. This study was carried out using models with methyl groups in place of cyclohexyl groups, an approximation that has been previously validated.[38] For the sake of simplicity we will not distinguish between the actual cyclohexyl-substituted complexes and their methyl-substituted models in the discussion that follows.

(33) Duckett, S. B.; Wood, N. J. *Coord. Chem. Rev.* **2008**, *252*, 2278.
(34) Pravica, M. G.; Weitekamp, D. P. *Chem. Phys. Lett.* **1988**, *145*, 255.
(35) Bowers, C. R.; Weitekamp, D. P. *J. Am. Chem. Soc.* **1987**, *109*, 5541.

(36) EXSY experiments are informative of an exchange process even when the signals of a molecule involved in the dynamic process are too broad to be unambiguously detected in the 1D spectrum.
(37) Aiming at comparing the isomerization rate in the presence and in the absence of free ligand, we have added 4 equiv of free $PHCy_2$ to a solution of complex **2**. Unfortunately, the free $PHCy_2$ immediately reacted with **2** to give the monobridged complex *cis*-[($PHCy_2$)$_2$(H)Pt(μ-PCy_2)Pt($PHCy_2$)(H)(κP-$P(O)Cy_2$)](*Pt*−*Pt*) (**5**), thus rendering the experiment uninformative.

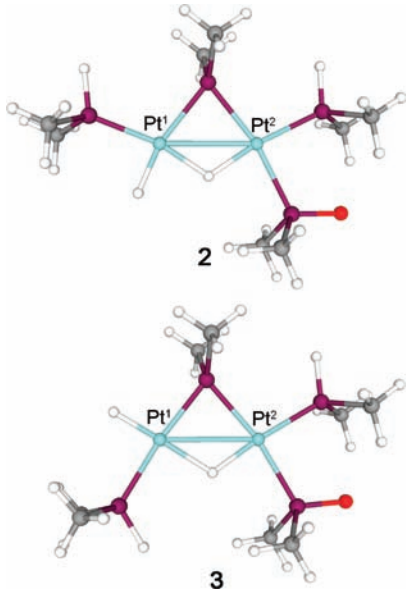

Figure 3. Optimized geometries of the *cis*- and *trans*-dihydrido complexes **2** and **3**: (cyan) platinum; (purple) phosphorus; (red) oxygen; (gray) carbon; (white) hydrogen.

Geometries and Thermodynamics. Geometry optimizations performed on the final *cis*- and *trans*-dihydrido complexes **2** and **3** gave the structures depicted in Figure 3, showing geometries very close to those determined experimentally and theoretically for the analogous species [(PHCy$_2$)(X)Pt(μ-PCy$_2$)(μ-H)Pt{κP-P(O)Cy$_2$}(PHCy$_2$)](*Pt*−*Pt*) (X = Cl, Br, I, PhO, PhS),[17] with the substituent X in place of the terminal hydride.

From a thermodynamic point of view the hydrogenation of **1** leading to the *cis*-dihydride **2** is exothermic, with an enthalpy gain of 13.9 kcal mol^{-1} in the gas phase (a higher value is calculated in polar solvent; see below) and a free energy gain of 4.5 kcal mol^{-1}. The significantly smaller ΔG value with respect to ΔH is attributable to the unfavorable entropy corrections due to the loss of a translational degree of freedom.

The *trans* isomer **3** is more stable than **2** by 4.8 kcal mol^{-1} in enthalpy and 5.3 kcal mol^{-1} in free energy in the gas phase (similar values are calculated in solution), in agreement with the experimentally found spontaneous isomerization of **2** to **3**.

Reaction Mechanism and Intermediates for the Hydrogenation Reaction of 1. Theoretical calculations have been initially focused on the detailed pathway of the hydrogenation reaction of **1**, through the characterization of the main intermediates and transition states and the calculation of the corresponding energy barriers. We first considered the formation of possible weak adducts between the H_2 molecule and the complex **1**. Three sites of complex **1** are in principle suitable for binding H_2, i.e., each of the two metal centers and the phosphinito oxygen might be able to polarize the incoming H_2 molecule.[39] Actually, several

(38) The reliability of this model in the reproduction of geometrical parameters has already been proved for complex **1** and derivatives, which have been structurally characterized by X-ray analysis, with calculated bond lengths and angles within 0.06 Å and 5°, respectively, from the experimental data. Gallo, V.; Latronico, M.; Mastrorilli, P.; Polini, F.; Re, N.; Englert, U. *Inorg. Chem.* **2008**, *47*, 4785 and Latronico, M.; Polini, F.; Gallo, V.; Mastrorilli, P.; Calmuschi-Cula, B.; Englert, U.; Re, N.; Repo, T.; Raisanen, M. *Inorg. Chem.* **2008**, *47*, 9779.

(39) Accordingly, a Mulliken gross atomic charge of −0.82 has been calculated for the oxygen in **1**. Gallo, V.; Latronico, M.; Mastrorilli, P.; Polini, F.; Re, N.; Englert, U. *Inorg. Chem.* **2008**, *47*, 4785.

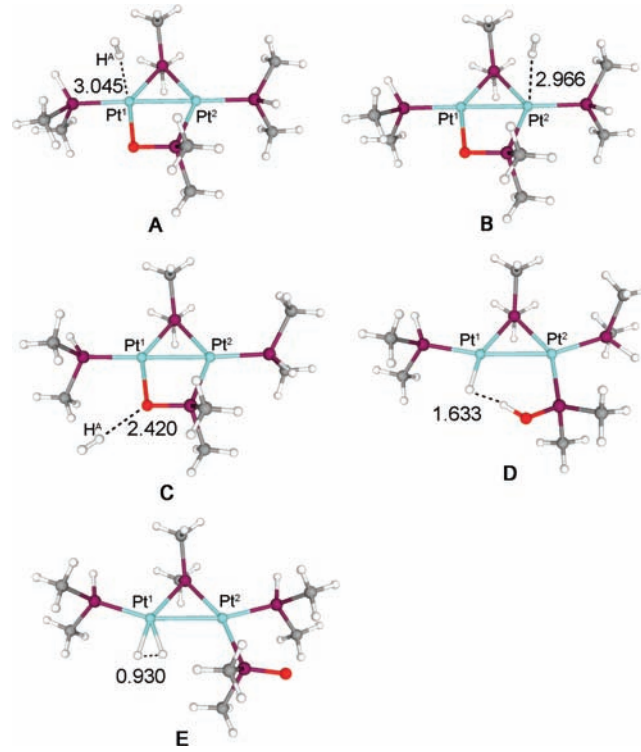

Figure 4. Optimized geometries of the intermediates **A**−**E**: (cyan) platinum; (purple) phosphorus; (red) oxygen; (gray) carbon; (white) hydrogen.

geometry optimizations starting from various orientations of H_2 with respect to each of these sites allowed us to locate three stable adducts (**A**−**C**, Figure 4). Two of them, **A** and **B**, derive from a weak η^1 coordination of the dihydrogen molecule to the Pt^1 or Pt^2 centers with the H−H axis almost perpendicular to the platinum coordination plane. The third adduct, **C**, shows the interaction between one atom of the H_2 and the phosphinito oxygen, with the H−H axis almost lying in the platinum coordination plane. The binding energies for all of these adducts are very low, being 1−2 kcal mol^{-1} with respect to **1** and the H_2 infinitely apart.

We then considered the possible pathways for the evolution of the initially formed hydrogen-bonded adducts **A** and **C** to the final dihydride product **2**, trying to identify the main intermediates and transition states.

This point was investigated by calculating the energy profiles for these pathways, taking the Pt^1−H^A distance as reaction coordinate. As far as **A** is concerned, the Pt^1−H^A distance was varied from 3.045 Å, the value in **A**, to 1.72 Å, the value in **2**, when the H_2 molecule is completely split, optimizing all the remaining geometrical parameters at each fixed value of the reaction coordinate, obtaining a maximum in the energy profile, ca. 17 kcal mol^{-1} above **A**. A maximum with similar energy and structure was obtained from the energy profile starting from **C** and using again the Pt^1−H^A distance as reaction coordinate. A transition state search starting from the geometry of this maximum allowed us to locate a structure, **TS$_1$**, 12.5 kcal mol^{-1} above **1** + H_2 in enthalpy (20.7 kcal mol^{-1} in free energy) with an imaginary frequency of 238 cm^{-1} and a normal mode corresponding to the H_2 splitting. The structure of **TS$_1$** is shown in Figure 5 and represents an early transition state in which (i) the H_2 molecule is only slightly elongated (R(H−H) = 0.77 Å), (ii) the two hydrogen atoms have approached the Pt^1 and O

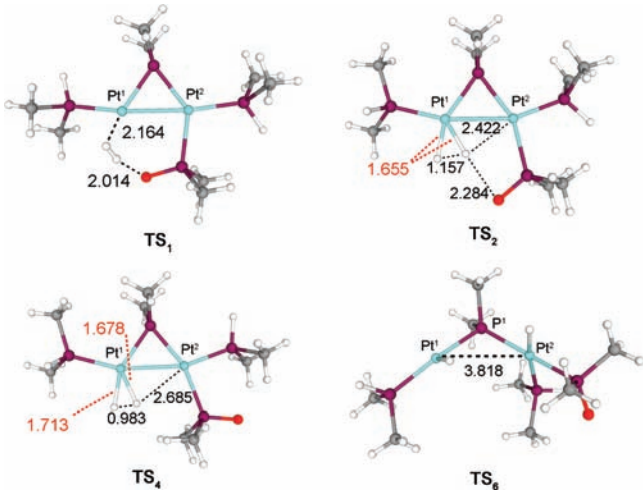

Figure 5. Optimized geometries of the transition states **TS₁**, **TS₂**, **TS₄**, and **TS₆**: (cyan) platinum; (purple) phosphorus; (red) oxygen; (gray) carbon; (white) hydrogen.

atoms with incipient formation of Pt−H and O−H bonds, and (iii) the phosphinito oxygen has almost detached the Pt^1 atom ($R(Pt^1-O) = 2.9$ Å).

The IRC calculations indicated that **TS₁** is connected backward to **A** and forward to a stable dinuclear [$(PHMe_2)(H)Pt(\mu$-$PMe_2)Pt(PHMe_2)\{\kappa^1P$-$P(OH)Me_2\}$](*Pt*−*Pt*) species, **D**, 10.7 kcal mol^{-1} below **1** + H_2, where the two split hydrogens are bound to Pt^1 and O atoms and interact with each other within a six-membered Pt^1−H···H−O−P−Pt^2 ring; see Figure 4. The geometries of the transition state and the results of the IRC calculations thus indicate that the transformation of **A** into **D** consists of a heterolytic splitting of the H_2 molecule assisted by the phosphinito oxygen.

It is worth noting that **D** has the same structure of the intermediates involved in the reaction of **1** with strong hydrohalic acids HX (X = Cl, Br, I), which have been identified by spectroscopic and theoretical studies as the dinuclear Pt−Pt species [$(PHCy_2)(X)Pt(\mu$-$PCy_2)Pt(PHCy_2)\{\kappa P$-$P(OH)Cy_2\}$]-(*Pt*−*Pt*), endowed with a six-membered Pt−X···H−O−P−Pt ring.[17] Given that such intermediates had been found to evolve to the bridging hydrido products [$(PHCy_2)(X)Pt(\mu$-$H)(\mu$-$PCy_2)Pt(PHCy_2)\{\kappa P$-$P(O)Cy_2\}$](*Pt*−*Pt*) through the migration of the O-bound hydrogen to the Pt−Pt bond, we considered the possibility that **D** evolved in the same way to give the dihydride product **2.** The enthalpy profile for the intramolecular rearrangement from **D** to **2** was obtained by varying the distance between the oxygen-bound hydrogen and the midpoint of the Pt−Pt bond (taken as the reaction coordinate) from 3.35 Å, the value in **D**, to 1.07 Å, the final value in **2**, and showed a maximum ca. 23 kcal mol^{-1} above **D**. A transition state search starting from the structure of the maximum gave a transition state, **TS₂**, 20.6 kcal mol^{-1} in enthalpy above **D** (in gas phase). The frequency analysis gave an imaginary frequency of 928 cm^{-1} corresponding to the expected normal mode. The geometry of **TS₂** (Figure 5) shows that the shifting hydrogen atom has almost detached from the O atom ($R(O-H) = 2.28$ Å) and significantly approached the Pt−Pt bond and in particular the Pt^1 atom ($R(Pt^1-H) = 1.66$ Å and $R(Pt^2-H) = 2.42$ Å); interestingly, this H atom is significantly close to the terminal H on Pt^1 ($R(H-H) = 1.16$ Å), indicating a role for a transient η^2-H_2-like structure in the stabilization of this transition state. Subsequent IRC calculations showed that **TS₂** is connected

Scheme 6. Enthalpy Profile (in the Gas Phase) for the Heterolytic Mechanism of Hydrogenation of **1**

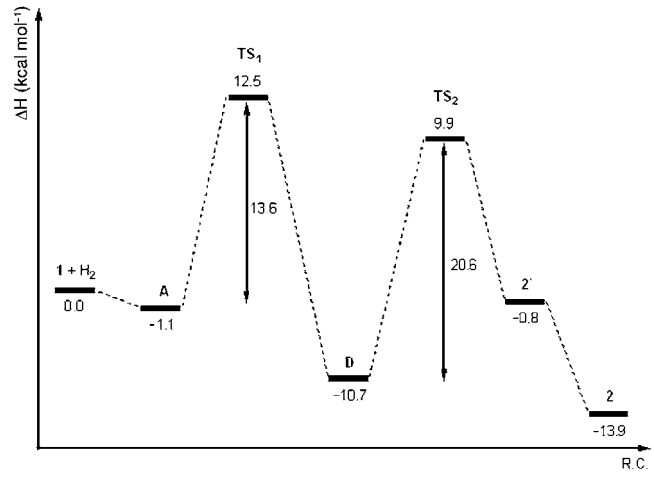

backward to **D** and forward to a conformer of **2** with the phosphinito oxygen synplanar to the bridging hydride, **2′**, 13.1 kcal mol^{-1} less stable than the lowest energy conformer with the oxygen atom antiperiplanar to the bridging hydride, and to which it is expected to evolve with a small barrier through rotation around the single Pt^2−P^3 bond (see Scheme 6).

These results show that the proton transfer from the phosphinito oxygen to the Pt−Pt bond is an exothermic process with a relatively low energy barrier, indicating that the intramolecular conversion of **D** to **2** occurs easily at room temperature or moderately low temperatures and is therefore in agreement with the experimental results, showing no evidence of the intermediate **D**.[40] The overall enthalpy profile calculated for the hydrogenation of **1** to **2** according to this heterolytic mechanism is reported in Scheme 6 and shows the highest barrier of 20.6 kcal mol^{-1} corresponding to the migration of the O-bound hydrogen in **D** to the Pt−Pt bond.

We also considered the alternative path consisting of the "side on" approach of H_2 to Pt^1 in **1** with formation of an early η^2-H_2 intermediate that leads to the final dihydride product via a homolytic H−H bond breaking. No stable η^2-dihydrogen complex could be optimized either when the phosphinito oxygen was bound to Pt^1 (due to the coordinative saturation of the metal center) or when the Pt^1−O bond was broken, but the O atom left around the Pt^1 center. In fact, in the latter case, any optimization attempt resulted in the collapse of the initially delineating η^2 structure into **D**, indicating that if the phosphinito oxygen is still close to the activated H_2 molecule, it invariably rips a hydrogen atom away, forming a O−H bond.

On the other hand, by approaching H_2 to **1** *after* breaking of the Pt^1−O bond and rotation of the $P(O)Cy_2$ group about the Pt^2—P^3 bond to put the oxygen atom antiperiplanar to Pt^1, a minimum corresponding to the η^2-dihydrogen complex **E** could be optimized (Figure 4), which was found 2.4 kcal mol^{-1} in enthalpy above **1** + H_2 (Scheme 7) and 13.1 kcal mol^{-1} above

(40) Previous calculations on the protonation of **1** with strong hydrohalic acids such as HCl[17] showed a significantly higher energy barrier for the isomerization of the six-membered platinacycle intermediate [$(PHCy_2)(Cl)Pt(\mu$-$PCy_2)Pt(PHCy_2)\{\kappa P$-$P(OH)Cy_2\}$](*Pt*−*Pt*) to the hydrido compound [$(PHCy_2)(X)Pt(\mu$-$PCy_2)(\mu$-$H)Pt(PHCy_2)\{\kappa P$-$P(O)Cy_2\}$]: 28 kcal mol^{-1} instead of 20.6 kcal mol^{-1}. The difference in value found for X = Cl, H could explain why the intermediate with X = Cl could be detected by NMR spectroscopy while that with X = H could not.

Scheme 7. Enthalpy Profile (in the Gas Phase) for the Homolytic Mechanism of Hydrogenation of **1**

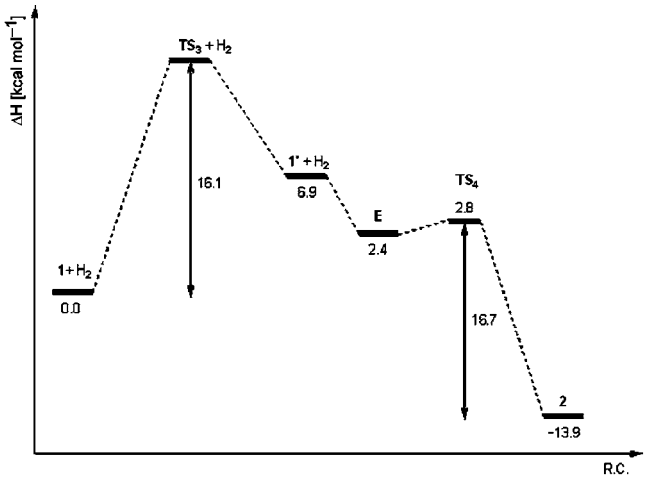

the intermediate **D**. The structure **E** corresponds to that of the nonclassical dihydrogen species **4** discussed above, with methyls replacing cyclohexyl groups.

The Pt^1 center in **E** shows a distorted-square-planar coordination geometry where the H_2 unit occupies the coordination site left vacant by the phosphinito oxygen with the H−H vector lying in the coordination plane and a moderately elongated H−H distance of 0.93 Å. However, the formation of **E** requires, prior to the H_2 binding, the complete detachment of the phosphinito oxygen from Pt^1 in **1** and the formation of the antiperiplanar conformer **1′**, which was found 6.9 kcal mol^{-1} higher in energy than **1**. Moreover, an energy scan from **1** to **1′** along the dihedral $Pt^1-Pt^2-P^3-O$ angle from 0 to 180° showed a maximum around 90°, with an energy 18 kcal mol^{-1} above **1** + H_2. Although we could not optimize a transition state for the **1** to **1′** conformer conversion starting from this geometry, because of the extreme flatness of the PES, a vibrational frequencies analysis led to only one imaginary frequency, indicating that this maximum is close to a first-order saddle point of the PES, as expected for a true transition state (**TS_3**). We could therefore approximately estimate zero-point and thermal corrections to this point, calculating an activation enthalpy of 16.1 kcal mol^{-1} for the formation of **1′** from **1**. We also searched for a transition state for the formation of **E** from **1** and H_2 whereby the dihydrogen moiety assists the rotation along the dihedral $Pt^1-Pt^2-P^3-O$ angle. However, all our attempts were unsuccessful; indeed, any transition state search starting with a dihedral Pt^1-Pt^2-P-O angle below 90° (i.e., left in the quadratic region of the synplanar conformer **1**) led to the transition state **TS_1** connected with **D**, while for dihedral angles around 90−100° the potential energy surface for the approach of H_2 to **1**, even in the presence of H_2, remains quite flat, preventing any transition state optimization. The formation of **E** from **1** and H_2 can therefore be reasonably described as occurring through the detachment of the phosphinito oxygen in **1** and the formation of the antiperiplanar conformer **1′**, followed by the easy coordination of H_2 to the coordinatively unsaturated Pt^1 atom, and **TS_3**, obtained as the maximum in the energy scan from **1** to **1′** evaluated before, 16.1 kcal mol^{-1} above **1**, is therefore a good approximation for the transition state from **1** to **E**. The binding energy of H_2 to the coordinatively unsatured Pt^1 center in **1′** is relatively low (4.5 kcal mol^{-1} in enthalpy) and without any significant energy barrier (an energy scan led to a maximum less than 1 kcal mol^{-1} above **1′** + H_2), leading to the overall enthalpy change of +2.4 kcal mol^{-1} for the formation of **E** from **1** and H_2 (a free energy change of 11.7 kcal mol^{-1}).

An energy scan for the oxidative addition of the η^2-bound H_2 in **E**, leading to **2**, showed that this is an easy process with a maximum of only 3 kcal mol^{-1}. We could locate a transition state for this step, **TS_4**, which has been confirmed by IRC calculations to connect **E** to **2**. A vanishingly low activation enthalpy of 0.4 kcal mol^{-1} (activation free energy of 0.5 kcal mol^{-1}) was calculated for this homolytic dihydrogen dissociation process.

The overall energy profile for this homolytic path is reported in Scheme 7 and shows an energy barrier of 16.1 kcal mol^{-1}, essentially corresponding to the breaking of the Pt−O bond in **1** and its rearrangement to the antiperiplanar conformer **1′**.

The comparison between the energy profiles for the heterolytic and homolytic pathways shows that, although the highest activation energies for the homolytic path are slightly lower, 16.1 vs 20.6 kcal mol^{-1}, the much lower barrier for the initial formation of **D** and the unfavorable requirement that the Pt−O must first break and then rotate to an antiperiplanar position forces the mechanism to follow the heterolytic pathway. This results is consistent with the experimental finding that no PHIP was observed in ^1H NMR spectra recorded during the hydrogenation of **1** carried out with para-H_2. The occurrence of the heterolytic rather than the homolytic mechanism is also supported by the positive KIE of 1.4 measured for the addition of H_2 to **1**; indeed, the barrier for the homolytic mechanism does not involve the breaking of the H_2 but that of the Pt−O bond and no KIE would be thus expected.

Heterolysis of H_2 mediated by transition-metal−ligand bonds have been recently reported for Rh−S,[41] Ir−S,[41b] and Ni−N[42] systems.

Mechanism of 2 → 3 Isomerization

All of the isomerization mechanisms proposed in Scheme 5 were addressed, and for each of them we calculated the geometries and the energies of all involved intermediates and transition states and estimated the corresponding energy barriers.

The dissociative mechanism (path i) was simulated through the dissociation of the P^2HCy_2 ligand from Pt^1, followed by the *cis* to *trans* isomerization of the tricoordinated Pt^1 center, with a T geometry, and the recoordination of the $PHCy_2$ ligand. As expected, the first step (i.e., dissociation of the P^2HCy_2) was calculated to be endothermic, by 32 kcal mol^{-1} (Scheme 8), and a linear transit calculation, using the Pt^1-P^2 distance as reaction coordinate, also showed that it is essentially barrierless. Moreover, upon the detachment of $PHCy_2$, the bridging hydride ligand spontaneously moves toward the neighboring terminal hydride, forming a Pt^1-bound η^2 dihydrogen complex, **F** (Figure S19).

The high energy of 32 kcal mol^{-1}, calculated for the detachment of the $PHCy_2$ ligand on Pt^1, and the formation of the dihydrogen complex, whose isomerization would require further unfavorable steps, allow us to discard this mechanism, in agreement with the experimental evidence showing no trace

(41) (a) Ienco, A.; Calhorda, M. J.; Reinhold, J.; Reineri, F.; Bianchini, C.; Peruzzini, M.; Vizza, F.; Mealli, C. *J. Am. Chem. Soc.* **2004**, *126*, 11954. (b) Ohki, Y.; Sakamoto, M.; Tatsumi, K. *J. Am. Chem. Soc.* **2008**, *130*, 11610–11611.
(42) Misumi, Y.; Seino, H.; Mizobe, Y. *J. Am. Chem. Soc.* **2009**, *131*, 14636.

Scheme 8. Enthalpy Profile (in the Gas Phase) for the Considered Pathways i−iii of the **2** → **3** Isomerization

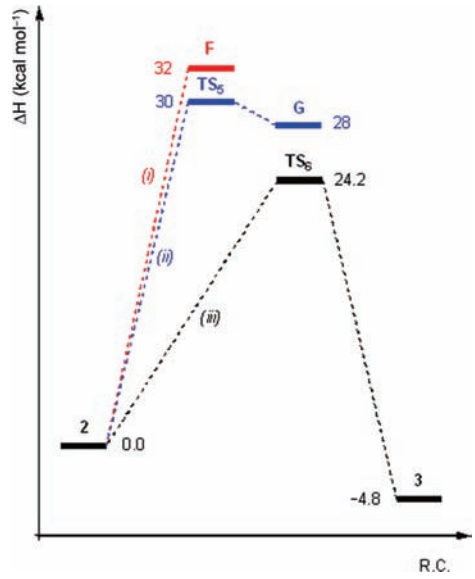

Scheme 9. Enthalpy Profiles in Solution for the Heterolytic Pathway of Hydrogenation

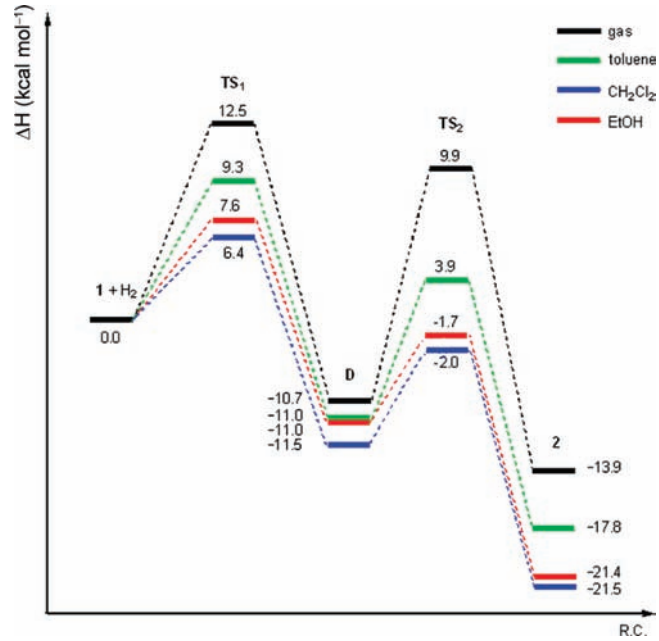

of free $PHCy_2$ and no exchange cross peak in the NMR spectra during the **2** → **3** isomerization.

We also considered path ii on the basis of the exchange between H^1 (the hydrogen originally bound to P^2) and the terminal hydride H^4 (Scheme 5). In spite of several attempts, no transition state was found for the concerted pathway consisting of the simultaneous transfer of H from the phosphane P^2 to Pt^1, *trans* to the bridging hydride, and from Pt^1 to P^2. On the other hand, we could characterize the asynchronous pathway consisting of an oxidative addition of the P^2-H^1 bond leading to a trihydride intermediate, **G** (Figure S20), and followed by a reductive elimination to **3** involving the newly formed terminal phosphanide and the *cis* hydrido ligand. **G** shows a pentacoordinated square-pyramidal Pt^1 center with an apical terminal phosphanide and two equatorial terminal hydrides and is a quite unstable species, 28.0 kcal mol^{-1} above **2**. We found a late transition state for this oxidative addition, $\mathbf{TS_5}$ (Figure S22), 30.0 kcal mol^{-1} above **2**. This large activation enthalpy allows us to discard this mechanism, in agreement with the experimental evidence indicating that the isomerization of **2**-d_2 led to a final **3**-d_2 complex showing no labeling of the coordinated P^2HCy_2 ligand.

We finally addressed the direct intramolecular isomerization via an out-of-plane slippage of the terminal hydride, mechanism iii. A transition state search along the direct pathway from **2** to **3** allowed us to localize a structure, $\mathbf{TS_6}$, 24.2 kcal mol^{-1} above **2**, which was confirmed by an IRC calculation to be directly connected to **2** and **3**. This TS showed a distorted geometry, showing broken Pt^1-Pt^2 and Pt^1-H^3 bonds, a shift of the phosphane ligand on Pt^1 from *cis* to *trans* position with respect to the bridging phosphanide, and a rotation of the Pt^1 and Pt^2 coordination planes around the P^1-Pt^1 and P^1-Pt^2 bonds (see Figure 5).

The enthalpy profiles for the above plausible pathways are reported in Scheme 8 and indicate that the direct pathway iii has the lowest activation enthalpy and is therefore expected to be the most favorable.[43] The calculated enthalpy barrier of 24.2 kcal mol^{-1} (2−3 kcal mol^{-1} lower in solution, see below) is consistent with the low rate experimentally observed for the **2** → **3** isomerization.

An intramolecular mechanism similar to pathway iii has been recently reported to account for the equivalence of terminal and bridging hydride ligands in the complex $[Pt_2(H)_2(\mu\text{-}H)(dppp)_2]^+$.[10k]

Solvent Effects. The hydrogenation mechanisms indicated by our calculations, either a heterolytic splitting of the H_2 molecule or a homolytic splitting requiring the previous breaking of the polar Pt−O bond, suggest that solvent effects could be very important, as experimentally observed, with polar solvents accelerating the hydrogenation reaction. We have thus evaluated the solvent effects on the energy profiles for both hydrogenation pathways and also for the favored direct mechanism of **2** → **3** isomerization, considering the three solvents experimentally employed and spanning a wide range of polarity: i.e., toluene ($\varepsilon = 2.4$), dichloromethane ($\varepsilon = 9.1$), and ethanol ($\varepsilon = 24.3$). The results are reported in Schemes 9−11 and indicate that an increase of the solvent polarity clearly favors both hydrogen splitting pathways, while it barely affects the isomerization process. Indeed, the thermodynamics of the hydrogenation reaction is favored by the polarity of the medium, with calculated reaction enthalpies of −13.9 kcal mol^{-1} (in gas phase), −17.8 kcal mol^{-1} (in toluene), −21.5 kcal mol^{-1} (in dichloromethane), and −21.4 kcal mol^{-1} (in ethanol). Moreover, the highest enthalpy barrier for the heterolytic pathway, the hydrogen

(43) An associative mechanism for the **2** → **3** isomerization, consisting of the addition of H_2 to **2** and subsequent reductive elimination of H_2 to give **3**, was also addressed. The addition of a further H_2 molecule to Pt^1 in **2** is a very slightly endothermic process, by 3 kcal mol^{-1}, and leads to a stable tetrahydrido species with three terminal hydride ligand on the octahedral Pt^1 center and a fourth hydride bridging the two metals, **H** (see Scheme S18). We found an early transition state for this oxidative addition, $\mathbf{TS_7}$, with a H−H distance of 1.02 Å, Pt^1-H distances of 1.97 and 1.98 Å, and a relatively high activation energy of 28 kcal mol^{-1} that renders this path unlikely. IRC calculations have shown that $\mathbf{TS_7}$ correlates backward with the most stable isomer of **H**, with the terminal $PHCy_2$ ligand in an axial position. An analogous transition state, $\mathbf{TS_8}$, 25 kcal mol^{-1} above **H**, was calculated for the final step, consisting of the reductive elimination of H_2 from **H**, involving the terminal hydride *cis* to the bridging hydride and leading to the final *trans*-dihydride **3**.

Scheme 10. Enthalpy Profiles in Solution for the Homolytic Pathway of Hydrogenation

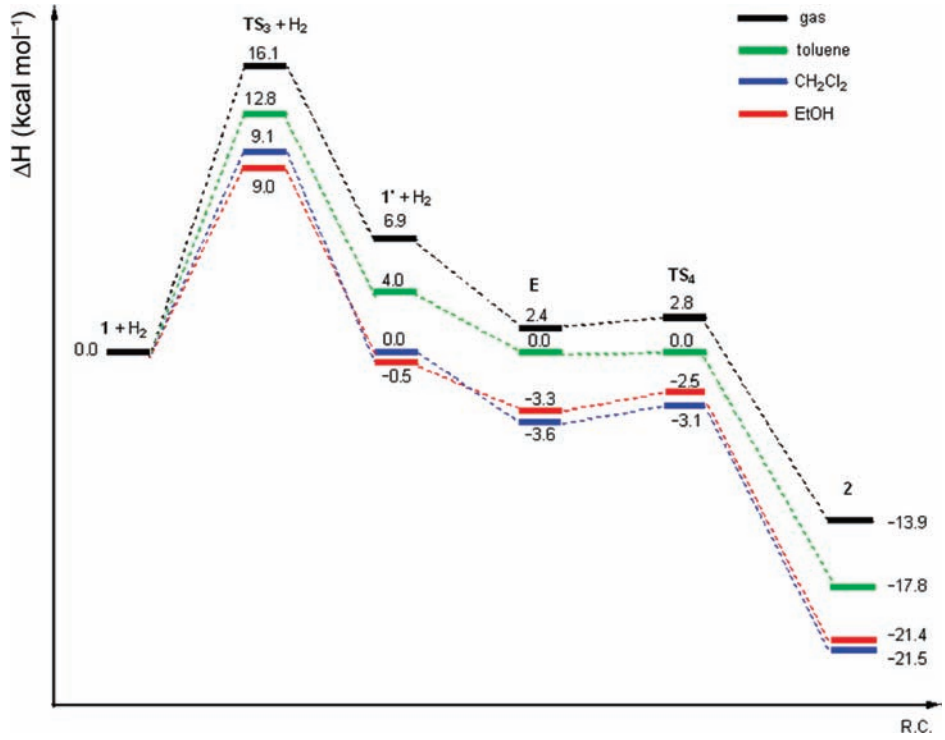

Scheme 11. Enthalpy Profiles in Solution for the Isomerization of **2** to **3**

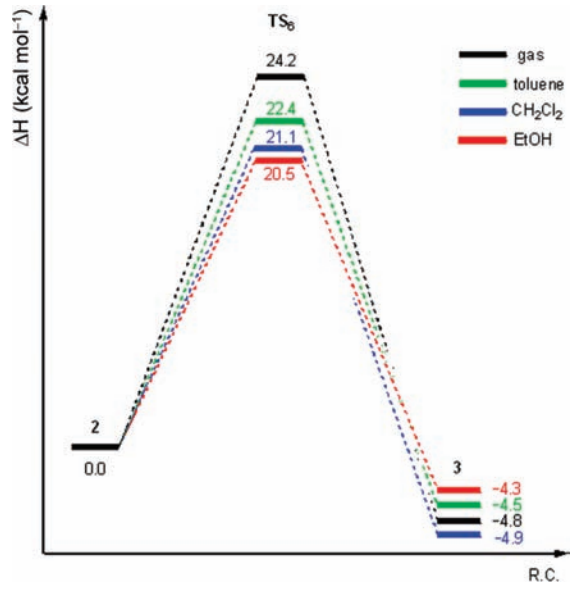

transfer from O to the Pt_2 core in **D**, decreases from 20.6 kcal mol^{-1} (in the gas phase) to 14.9 kcal mol^{-1} (in toluene), 9.5 kcal mol^{-1} (in dichloromethane), and 9.3 kcal mol^{-1} (in ethanol); see Scheme 9. Scheme 10 shows that, analogously, also the highest enthalpy barrier for the homolytic pathway, the cleavage of the Pt−O bond in **1**, decreases from 16.1 kcal mol^{-1} (in the gas phase) to 12.8 kcal mol^{-1} (in toluene), 9.1 kcal mol^{-1} (in dichloromethane) and 9.0 kcal mol^{-1} (in ethanol), still remaining always higher than that for the heterolytic pathway.

On the other hand, the thermodynamics of the isomerization is poorly affected, the isomerization enthalpy passing from −4.8 kcal mol^{-1} (in the gas phase) to −4.5 kcal mol^{-1} (in toluene), −4.9 kcal mol^{-1} (in dichloromethane) and −4.3 kcal mol^{-1} (in ethanol), and the isomerization activation enthalpy for the most favored direct isomerization pathway iii decreases only very slightly, being 24.2 kcal mol^{-1} (in the gas phase), 22.4 kcal mol^{-1} (in toluene), 21.1 kcal mol^{-1} (in dichloromethane), and 20.5 kcal mol^{-1} (in ethanol) (Scheme 11). These results are in agreement with the experimental findings, showing that the hydrogenation of **1** to **2** is complete in 6 h in toluene, 20 min in dichloromethane, and 5 min in ethanol, while the times required for a complete isomerization in the three solvents are roughly the same.

A growing body of data indicate that alcohols can act as promoters of heterolytic H_2 cleavage in several metal-catalyzed hydrogenation reactions, and this effect has been attributed either to the polarization of the cleaving H_2 moiety in the transition state through a hydrogen bond or to the direct involvement of the alcohol oxygen in a proton-hopping mechanism.[44] For this reason we performed the calculations on the heterolytic splitting of H_2 by **1** also including one explicit EtOH molecule, considering either a simple hydrogen-bond polarization of the previously characterized transition state (path a) or a proton-hopping mechanism through an eight-membered-ring transition state (path b). Scheme 12 shows paths a and b for the reaction of **1** with D_2 (rather than H_2) that leads to different isotopologues of the intermediate **D** and of the product **2**, depending on the followed path: path a gives **D**-d_2 (as EtOH adduct) and **2**-d_2, whereas path b gives **D**-*dh* (as the EtOD adduct) and **2**-*dh*.

Our calculations showed the formation of a quite stable adduct of **1** and EtOH, **1**·EtOH, with a binding enthalpy of 6.2 kcal mol^{-1}. In the same way observed for **1**, **1**·EtOH forms a labile adduct with the approaching H_2 molecule, **A**·EtOH, showing a η^1 coordination to Pt^1, that has been characterized by a negligibly

(44) (a) Sandoval, C. A.; Ohkuma, T.; Muñiz, K.; Noyori, R. *J. Am. Chem. Soc.* **2003**, *125*, 13490. (b) Casey, C. P.; Johnson, J. B.; Singer, S. W.; Cui, Q. *J. Am. Chem. Soc.* **2005**, *127*, 3100. (c) Comas-Vives, A.; Arellano-Gonzàles, C.; Corma, A.; Iglesias, M.; Sànchez, M.; Ujaque, G. *J. Am. Chem. Soc.* **2006**, *128*, 4756.

Scheme 12. Ethanol-Catalyzed D_2 Heterolytic Splitting through (a) Polarization of the Breaking H_2 Moiety in the Transition State by Formation of a Hydrogen Bond and (b) a Proton-Hopping Mechanism via an Eight-Membered-Ring Transition State

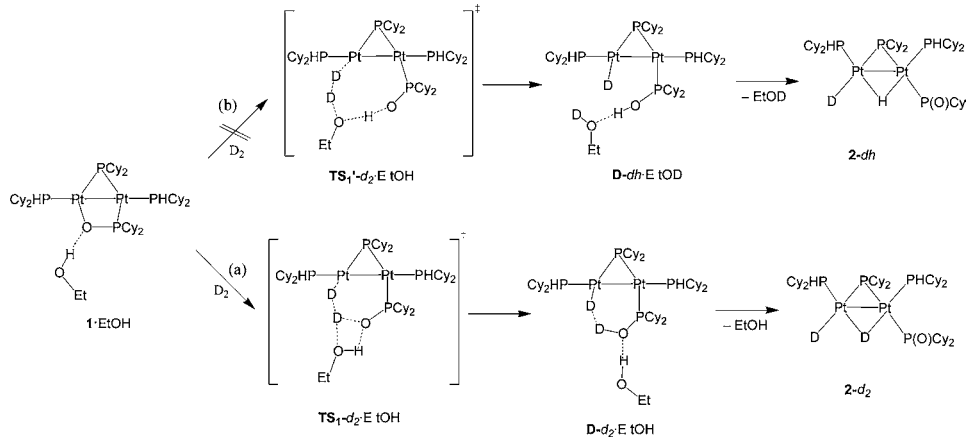

small binding enthalpy (in the gas phase). The transition state **TS$_1$**·EtOH was found for the phosphinito-assisted heterolytic splitting of H_2, which shows a geometry close to that found in the absence of ethanol (**TS$_1$**) with the EtOH molecule involved in two hydrogen bonds: one to the phosphinito oxygen and the other one to the adjacent H atom (see path a in Scheme 12). An activation enthalpy of 3.4 kcal mol^{-1} was calculated (after the inclusion of the continuum solvent effect) which was 3.0 kcal mol^{-1} lower than the value calculated without the inclusion of an explicit EtOH molecule (6.4 kcal mol^{-1}, see Scheme 9 and Table S16d). In spite of several efforts, no transition state could be found corresponding to path b in Scheme 12. An energy scan along the distance between the ethanol oxygen and the adjacent hydrogen atom of H_2, from 2.4 Å (the value in **A**·EtOH) to 1.01 Å (the value in EtOH), led to a maximum ca. 27 kcal mol^{-1} above **A**·EtOH, suggesting that path b requires indeed a high activation energy. The unlikeliness of path b has been experimentally confirmed by the outcome of the reaction of **1** with D_2 in EtOH, which gave exclusively the **2**-d_2 isotopologue (instead of **2**-*dh*, the product of path b; see Scheme 12). These results indicate that ethanol favors H_2 heterolytic splitting through both bulk polarization and specific hydrogen bond interactions, both effects stabilizing the transition state **TS$_1$**. We also calculated the transition state, **TS$_2$**·EtOH, for the subsequent rearrangement from **D** to **2** by explicitly including an EtOH molecule (hydrogen bonded to the phosphinito oxygen). It was found 11.1 kcal mol^{-1} higher in enthalpy with respect to **D**, thus indicating that the activation enthalpies do not change significantly on passing from the continuum solvent model to the explicit consideration of one EtOH molecule.

Reversibility of the Hydrogenation. The dehydrogenation of the hydride products **2** and **3** to give **1** was also investigated. A careful analysis of the free energies for the hydrogenation of **1** to **2** in the gas phase, and of the isomerization of **2** to **3** (see Scheme 13), showed that the free energy of **2** is only 4.5 kcal mol^{-1} below **1** and therefore an equilibrium between **1** and **2** could be operative, thus giving a rationale for the observed reversibility of the hydrogenation of **1** under reduced pressure.

When we consider the mechanism of this dehydrogenation reaction on the basis of the calculated energy profiles (see Schemes 6 and 7) we should take into account that the high-vacuum conditions could change the favored hydrogenation pathway—the heterolytic splitting through **D**—when the reaction is carried out in the reverse direction. Indeed, a lower activation enthalpy has been calculated for the formation of the η^2-dihydrogen adduct **E**—the intermediate of the homolytic splitting pathway—than for the formation of **D** (16.7 kcal mol^{-1} instead of 23.8 kcal mol^{-1}), and moreover, due to the lability of the η^2-bound H_2 molecule, **E** is expected to easily lose dihydrogen under vacuum conditions. The activation enthalpy for the complete dehydrogenation of **2** must, however, include also the binding enthalpy of H_2 in **E** (4.5 kcal mol^{-1}) and reaches a value of 21.2 kcal mol^{-1}, comparable to that for the isomerization of **2** to **3** (24.2 kcal mol^{-1}), so that the processes of dehydrogenation and of isomerization are expected to compete, as experimentally observed.

Scheme 13. Free Energies of the Hydrogenation Products

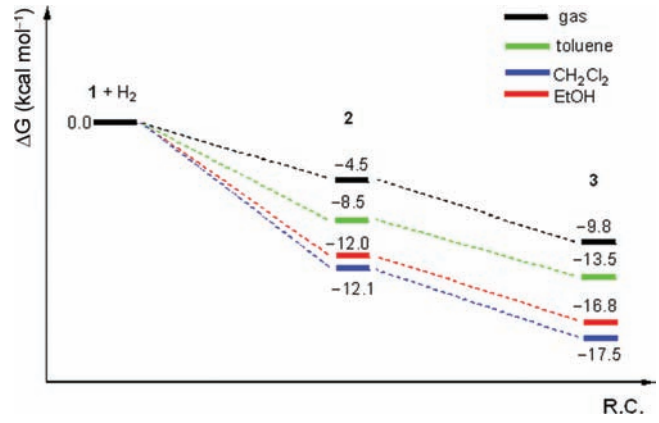

On the other hand, the hydrogenation in solution, especially in the polar solvents CH_2Cl_2 and ethanol, is much more exergonic (see Scheme 13) by about 12 kcal mol^{-1} from **2** and 17 kcal mol^{-1} from **3** and the reverse reaction can be ruled out in agreement with the experimental findings.

H/D Exchange and Isotopic Kinetic Effect. The hydride ligands in **2** easily undergo intermolecular exchange with D_2 under atmospheric pressure at room temperature both in solution and in the solid state. The nonclassical dihydrogen complex [(PHCy$_2$)(η^2-H$_2$)Pt(μ-PCy$_2$)Pt(PHCy$_2$){κP-P(O)Cy$_2$}](*Pt*−*Pt*) (**4**) can be relatively easily accessed from **2** at room temperature and is therefore a good candidate as the intermediate in the hydride exchange process by either D_2 or a second H_2 molecule. Indeed, once **4** is formed, the labile η^2-bound dihydrogen ligand can be easily lost and substituted by an incoming D_2 (or H_2) molecule, which then undergoes an oxidative addition to **2**-d_2 (or back to **2**). The latter step has been already addressed within the homolytic

Scheme 14. Proposed Mechanism for the H/D Exchange of **2**

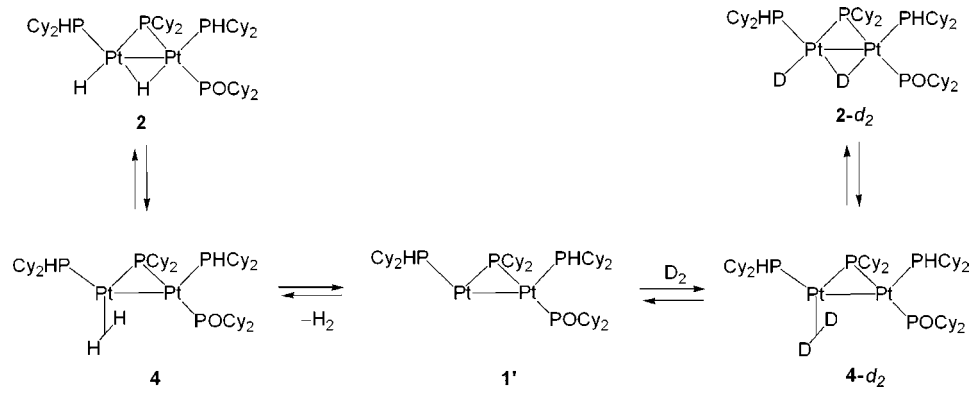

Scheme 15. Enthalpy Profile (in the Gas Phase) for the Hydrogen Exchange in **2**

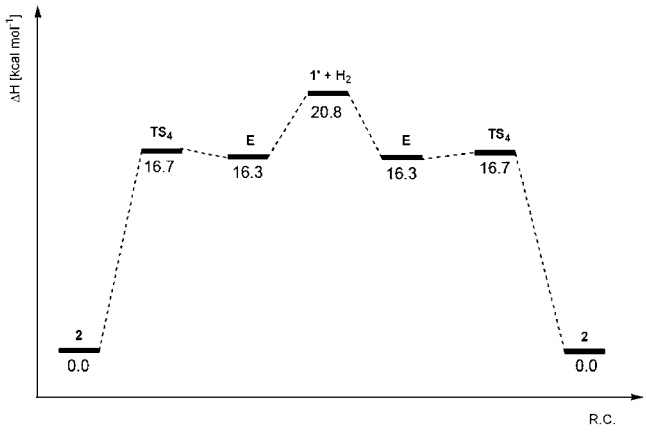

mechanism for the hydrogenation of **1** (see Scheme 7) and has been shown to pass through a low-energy transition state, **TS_4**, with a negligible activation enthalpy (0.4 kcal mol^{-1}). We have also considered the H_2 substitution process in **E** (the model for **4** used in DFT calculations), which follows a dissociative mechanism with no significant transition state for the H_2 detachment from **E** and for the D_2 (or H_2) rebinding. The overall mechanism is reported in Scheme 14, and the enthalpy profile in Scheme 15 shows that the highest barrier for this exchange process is 20.8 kcal mol^{-1} in the gas phase (21−22 kcal mol^{-1} in solution depending on the solvent). This activation energy value is sufficiently low to allow an easy deuterium exchange at room temperature but high enough to make the fluxionality process relatively slow on the NMR time scale, thus allowing us to observe two separate signals for the terminal and bridging hydride ligands on the ^1H NMR spectra of **2** at room temperature.

Finally, we calculated the KIE for the hydrogenation reaction, on the basis of the free energy profile of the stepwise heterolytic mechanism (see details in the Experimental Section) and found a value of 1.1. On the other hand, no KIE would be expected for the homolytic mechanism, because the barrier does not involve the breaking of the H_2 but that of the Pt−O bond.

The calculated value for the heterolytic mechanism (k_H/k_D = 1.1) is qualitatively consistent with the rough experimental value of 1.4, further supporting such a mechanism.

Conclusions

The Pt−O fragment of **1** constitutes the reaction core of the molecule, capable of activating H_2 under ambient conditions. In fact, whatever geometry the approaching dihydrogen adopts (i.e., side-on or end-on), the interaction of H_2 with Pt^1 gives directly the labile intermediate **D**, which evolves into **2** by H transfer from the PO to the Pt−Pt bond. A relatively low activation enthalpy (14.9 kcal mol^{-1} in toluene and 9.5 kcal mol^{-1} in dichloromethane) has been found for this heterolytic H_2 splitting process. The lack of formation of a nonclassical H_2 complex in the **1** → **2** transformation is related to the presence of the Pt-bonded oxygen atom, which acts as a Lewis base toward the activated H_2, ripping one of the two H atoms as soon as H_2 approaches the Pt^1 center. Thus, a mandatory condition for the formation of the σ-bonded H_2 complex **4** is that the phosphinito oxygen stays in an antiperiplanar position with respect to Pt^1, a situation fulfilled in the *cis*-dihydride **2**. Hence, complex **4** is an intermediate in the dehydrogenation of **2** to **1.** The species **4** is also involved in the intramolecular exchange between terminal and bridging hydrides in **2**, as well as in the intermolecular H_2/D_2 exchange leading from **2** to **2**-d_2 and vice versa. Experimental and DFT methods allowed us to determine that path iii of Scheme 5 is followed in the **2** → **3** isomerization: i.e., the intramolecular mechanism passing through the transition state **TS_6** with an activation enthalpy of 24.2 kcal mol^{-1}. Further evidence of the fact that the H_2 addition does not involve a σ-H_2 complex was also obtained by para-H_2 experiments, where the PHIP absence is in full agreement with a heterolytic process. As expected for a heterolytic mechanism of H_2 activation, a strong solvent effect was experimentally found and theoretically justified by DFT. The addition of hydrogen to **1** under mild conditions (1 bar, 298 K) suggests future applications of **1** as a hydrogenation catalyst. Complex **1** might also represent a good model for hydrogen storage.

Experimental Section

Complex **1** was prepared as described in ref 9. A stream of dry D_2 was obtained by the action of Na on CH_3OD and purified by passage through a cold (liquid nitrogen) trap that retained the methanol and an H_2SO_4 trap that retained the moisture. Dicyclohexylphosphane was obtained commercially (Strem) and used under N_2. The high-purity deuterated solvents CD_2Cl_2, benzene-d_6, and ethanol-d_6 were purchased from EURISO-TOP (Saint Aubin, France) and used without further purification. The solvents used were freshly distilled and oxygen-free. C, H elemental analyses were carried out on a Carlo Erba EA1108 CHNS-O elemental analyzer. Infrared spectra were recorded on a Bruker Vector 22 spectrometer. Mass spectrometry analyses were performed using a time-of-flight mass spectrometer equipped with an electrospray ion source (Bruker microTOF). The analyses were carried out in the positive ion mode. The sample solutions were introduced by continuous infusion with the aid of a syringe pump at a flow rate of 180 μL/min. The instrument was operated at end plate offset

−500 V and capillary −4500 V. The nebulizer pressure was 1.5 bar (N_2) and the drying gas (N_2) flow 10 L/min. Capillary exit and skimmer 1 were 120 and 40 V, respectively. The drying gas temperature was set at 220 °C. The software used for the simulations was Bruker Daltonics DataAnalysis (version 3.3).

NMR spectra were recorded on a Bruker Avance 400 spectrometer; frequencies are referenced to Me_4Si (^1H), 85% H_3PO_4 (^{31}P), and H_2PtCl_6 (^{195}Pt). The coupling constants not directly extractable from the one-dimensional spectra were obtained and attributed by the tilts of the multiplets due to the "passive" nuclei[45] in $^1H-^{31}P$ HMQC and $^1H-^{195}Pt$ HMQC spectra. The ^1H NOESY-EXSY spectrum reported in Figure 2 was recorded using a mixing time of 600 ms. The ^2H NMR spectra were recorded by running the instrument unlocked.

Computational Details. All calculations were carried out at density functional theory level by using Jaguar 6 programs.[46] Geometry optimization and linear transit calculations have been performed by using the B3LYP functional[47] with the 6-311G** basis set for main-group elements (C, O, H) and by the Los Alamos LACV3P*[48] basis for Pt, including relativistic effective core potentials. IRC calculations[49] have been further carried out in order to assess the reactant and product configurations, which are connected through the involved TS. Subsequent vibrational frequency calculations based on analytical second derivatives at the B3LYP/LACV3P** level of theory have been carried out to confirm the nature of the local minima and transition state and to compute the zero point energy (ZPE) and vibrational entropy corrections at 298.15 K. Solvation free energies were evaluated by a self-consistent reaction field (SCRF) approach[50] based on accurate numerical solutions of the Poisson−Boltzmann equation.[51] Solvation calculations were carried out on the gas-phase geometry at the B3LYP/LACV3P** level of theory by simulating the reaction field of three solvents: toluene ($\varepsilon = 2.4$ and $\sigma = 2.762$ Å; dielectric constant and solvent radius, respectively), dichloromethane ($\varepsilon = 8.93$ and $\sigma = 2.670$ Å), and ethanol ($\varepsilon = 24.3$ and $\sigma = 2.262$ Å). The activation and reaction enthalpies in solution have been estimated by adding the solvation free energy to the corresponding gas-phase enthalpy. Their variations are expected to be reliable, since the solvation entropy variations are likely to be negligible.

The kinetic isotope effect (KIE) of the hydrogenation reaction was determined using the DFT data based on the semiclassical model.[52] This model uses Eyring's equation for the reaction rate constant k_r of an elementary step as a function of temperature T:

$$k_r = \frac{k_B T}{h} e^{-\Delta G^{\ddagger}/RT}$$

where $\Delta G^{\ddagger}$ is the free energy of activation, k_B is the Boltzmann constant, and h is the Planck constant.

On the basis of this equation, the KIE of such an elementary step can be calculated from the free energies of activation of the deuterium substituted and reference systems as

$$KIE_r = k^H/k^D = e^{-(\Delta G^{\ddagger}_H - \Delta G^{\ddagger}_D)/RT}$$

A two-step process such as the hydrogenation of **1** occurring via the heterolytic mechanism in Scheme 6 can be described by the following steady-state analysis:

$$\mathbf{A} \underset{k_{-1}}{\overset{k_1}{\rightleftarrows}} \mathbf{D} \xrightarrow{k_2} \mathbf{2}$$

where an irreversible hydrogen shift from O to the Pt−Pt bond was assumed, consistent with the experimental evidence and the calculated profile in CH_2Cl_2 solution, and the observed rate constant k_{obs} can be written as

$$k_{obs} = \frac{k_1 k_2}{k_{-1} + k_2}$$

The observed KIE can be therefore expressed as

$$KIE_{obs} = \frac{k^H_{obs}}{k^D_{obs}} = \frac{k^H_1 k^H_2}{k^H_{-1} + k^H_2} \frac{k^D_{-1} + k^D_2}{k^D_1 k^D_2} = KIE_1 KIE_2 \frac{k^D_{-1} + k^D_2}{k^H_{-1} + k^H_2}$$

***cis*-[(PHCy$_2$)(H)Pt(μ-PCy$_2$)(μ-H)Pt(PHCy$_2$){κ*P*-P(O)Cy$_2$}]-(*Pt*−*Pt*) (2).** In a Schlenk tube containing a dichloromethane solution of **1** (80 mg, 0.066 mmol in 0.8 mL), H_2 was bubbled under ambient conditions at a flow rate of 0.8 mL/min. After 20 min the solvent was removed under reduced pressure. The pale yellow residue was not kept under high vacuum in order to avoid its transformation into **1**. Yield: 77.8 mg (97%). The complex is soluble in halogenated solvents, in aromatic solvents, and in ethanol; it is poorly soluble in *n*-hexane.

IR (KBr, pellet): 2923 (s); 2848 (s); 2658 (w); 2301 (w), ν(P−H); 1935 (m), ν(H−Pt); 1636 (w), ν(Pt−H−Pt); 1447 (s); 1342 (w); 1328 (w), 1292 (w); 1265 (m); 1190 (m); 1176 (m); 1105 (m); 1049 (s), ν(P═O); 1002 (s); 916 (m); 863 (m); 848 (m); 818 (m); 736 (s); 538 (m); 516 (s); 456 (m); 414 (w); 375 (w) cm^{-1}. ^1H NMR (C_6D_6, 298 K): δ 5.34 (m, H(1), $^1J_{H(1),P(2)} = 370$ Hz, $^2J_{H(1),Pt(1)} = 64$ Hz), 5.02 (m, H(2), $^1J_{H(2),P(4)} = 340$ Hz, $^2J_{H(2),Pt(2)} = 52$ Hz), −0.86 (m, H(4), $^2J_{H(4),P(1)} = 122$ Hz, $^2J_{H(4),P(2)} = 27$ Hz, $^1J_{H(4),Pt(1)} = 948$ Hz), −3.63 (m, H(3), $^2J_{H(3),P(1)} = 16$ Hz, $^2J_{H(3),P(2)} = 71$ Hz, $^2J_{H(3),P(3)} = 10$ Hz, $^2J_{H(3),P(4)} = 68$ Hz, $^1J_{H(3),P(t1)} = 544$ Hz, $^1J_{H(3),Pt(2)} = 591$ Hz) ppm. $^{31}P\{^1H\}$ NMR (CD_2Cl_2, 298 K): δ 119.2 (dd, P(1), $^2J_{P(1),P(3)} = 245$ Hz, $^2J_{P(1),P(2)} = 11$ Hz, $^1J_{P(1),P(t1)} = 1611$ Hz, $^1J_{P(1),Pt(2)} = 1120$ Hz), 75.3 (dd, P(3), $^2J_{P(3),P(1)} = 245$ Hz, $^2J_{P(3),P(4)} = 22$ Hz, $^1J_{P(3),Pt(2)} = 2483$ Hz), 11.3 (br, P(4), $^2J_{P(4),P(1)} = 11$ Hz, $^3J_{P(4),P(2)} = 49$ Hz, $^2J_{P(4),P(3)} = 21$ Hz, $^1J_{P(4),Pt(2)} = 3917$), 9.5 (dd, P(2), $^2J_{P(2),P(1)} = 11$ Hz, $^3J_{P(2),P(4)} = 49$ Hz, $^1J_{P(2),Pt(1)} = 3944$ Hz, $^2J_{P(2),Pt(2)} = 202$ Hz) ppm. $^{195}Pt\{^1H\}$ NMR (C_6D_6, 298 K): δ −5901 (dddd, Pt(1), $^1J_{Pt(1),P(1)} = 1601$ Hz, $^1J_{Pt(1),P(2)} = 3967$ Hz, $^2J_{Pt(1),P(3)} = 36$ Hz, $^2J_{Pt(1),P(4)} = 201$ Hz, $^1J_{Pt(1),Pt(2)} = 608$ Hz), −5584 (dddd, Pt(2), $^1J_{Pt(2),P(1)} = 1110$ Hz, $^2J_{Pt(2),P(2)} = 204$ Hz, $^1J_{Pt(2),P(3)} = 2486$ Hz, $^1J_{Pt(2),P(4)} = 3896$ Hz, $^1J_{Pt(2),Pt(1)} = 608$ Hz) ppm.

***trans*-[(H)(PHCy$_2$)Pt(μ-PCy$_2$)(μ-H)Pt(PHCy$_2$){κ*P*-P(O)Cy$_2$}](*Pt*−*Pt*) (3).** In a Schlenk tube containing a dichloromethane solution of **1** (60 mg, 0.05 mmol in 0.8 mL), H_2 was bubbled under ambient conditions at a flow rate of 0.8 mL/min for 30 min. The solution was left to stand 3 days at room temperature; then the solvent was removed under high vacuum and pure **3** was obtained as a yellow solid. Yield: 58.9 mg (98%). The complex is soluble in halogenated solvents, in aromatic solvents, and in ethanol; it is insoluble in *n*-hexane.

Anal. Calcd for $C_{48}H_{92}OP_4Pt_2$: C, 48.1; H, 7.73. Found: C, 47.9; H, 7.82. HR ESI-MS: exact mass for $C_{50}H_{95}NOP_4Pt_2$ *m*/*z* 1198.5394; measured *m*/*z* 1199.5498 (M + H)$^+$. IR (KBr, pellet): 2931 (s); 2849 (s); 2653 (w); 2305 (m), ν(P−H); 2089 (m), ν(H−Pt); 1980 (w); 1824 (w); 1711 (w); 1635 (w), ν(Pt−H−Pt); 1597 (w); 1447 (s); 1342 (m); 1327 (m), 1292 (m); 1263 (s); 1191 (m); 1177 (m); 1107 (s); 1076 (s); 1045 (s), ν(P═O); 1002 (s), 916 (m); 886 (m); 849 (m); 817 (m); 735 (m); 668 (w); 575 (w); 521 (m); 467 (m);

(45) Carlton, L. *Bruker Rep.* **2000**, *148*, 28.
(46) Jaguar, version 6.0; Schrödinger, LLC, New York, 2005.
(47) (a) Becke, A. D. *J. Chem. Phys.* **1993**, *98*, 5648. (b) Lee, C. T.; Yang, W. T.; Parr, R. G. *Phys. Rev.* **1988**, *37*, 785.
(48) (a) Hay, P. J.; Wadt, W. R. *J. Chem. Phys.* **1985**, *82*, 270. (b) Wadt, W. R.; Hay, P. J. *J. Chem. Phys.* **1985**, *82*, 284. (c) Hay, P. J.; Wadt, W. R. *J. Chem. Phys.* **1985**, *82*, 299.
(49) (a) Gonzalez, C.; Schegel, H. B. *J. Chem. Phys.* **1989**, *90*, 2154. (b) Gonzalez, C.; Schegel, H. B. *J. Chem. Phys.* **1990**, *94*, 5523.
(50) (a) Tomasi, J.; Persico, M. *Chem. Rev.* **1994**, *94*, 2027. (b) Cramer, C. J.; Truhlar, D. G. *Chem. Rev.* **1999**, *99*, 2161.
(51) (a) Tannor, D. J.; Marten, B.; Murphy, R. B.; Friesner, R. A.; Sitkoff, D.; Nicholls, A.; Ringnalda, M. N.; Goddard, W. A., III; Honig, B. *J. Am. Chem. Soc.* **1994**, *116*, 11875. (b) Marten, B.; Kim, K.; Cortis, C.; Friesner, R. A.; Murphy, R. B.; Ringnalda, M. N.; Sitkoff, D.; Honig, B. *J. Phys. Chem.* **1996**, *100*, 11775.
(52) Melander, L.; Saunders, W. H., Jr. *Reaction Rates of Isotopic Molecules*; Robert E. Krieger Publishing: Malabar, FL, 1987.

453 (m); 416 (w); 382 (w) cm^{-1}. ^1H NMR (C_6D_6, 298 K): δ 5.29 (m, H(2), $^1J_{H(2),P(4)} = 371$ Hz, $^2J_{H(2),Pt(2)} = 42$ Hz), 4.80 (m, H(1), $^1J_{H(1),P(2)} = 318$ Hz, $^2J_{H(1),Pt(1)} = 16$ Hz), −5.29 (m, H(4), $^2J_{H(4),P(1)} = 4$ Hz, $^2J_{H(4),P(2)} = 26$ Hz, $^3J_{H(4),P(3)} = 5$ Hz, $^3J_{H(4),P(4)} = 35$ Hz,$^1J_{H(4),Pt(1)} = 1499$ Hz, $^2J_{H(4),Pt(2)} = 118$ Hz), −5.40 (m, H(3), $^2J_{H(3),P(1)} = 18$ Hz, $^2J_{H(3),P(2)} = 11$ Hz, $^2J_{H(3),P(3)} = 16$ Hz, $^2J_{H(3),P(4)} = 88$ Hz,$^1J_{H(3),Pt(1)} = 364$ Hz, $^1J_{H(3),Pt(2)} = 632$ Hz) ppm. $^{31}P\{^1H\}$ NMR (C_6D_6, 298 K): δ 134.5 (pseudo td, P(1), $^2J_{P(1),P(2)} = 257$ Hz, $^2J_{P(1),P(3)} = 263$ Hz, $^2J_{P(1),P(4)} = 16$ Hz, $^1J_{P(1),Pt(1)} = 2066$ Hz, $^1J_{P(1),Pt(2)} = 1193$ Hz), 83.3 (d, P(3), $^2J_{P(3),P(1)} = 263$ Hz, $^1J_{P(3),Pt(2)} = 2599$ Hz), 14.4 (d, P(2), $^2J_{P(2),P(1)} = 257$ Hz, $^1J_{P(2),Pt(1)} = 2564$ Hz), 11.5 (br, P(4), $^2J_{P(4),P(1)} = 16$ Hz,$^2J_{P(4),Pt(1)} = 170$ Hz, $^1J_{P(4),Pt(2)} = 3756$ Hz) ppm. $^{195}Pt\{^1H\}$ NMR (C_6D_6, 298 K): δ −5947 (dddd, Pt(1), $^1J_{Pt(1),P(1)} = 2068$ Hz, $^1J_{Pt(1),P(2)} = 2561$ Hz, $^2J_{Pt(1),P(3)} = 60$ Hz, $^2J_{Pt(1),P(4)} = 170$ Hz, $^1J_{Pt(1),Pt(2)} = 1340$ Hz), −5643 (dddd, Pt(2), $^1J_{Pt(2),P(1)} = 1193$ Hz, $^2J_{Pt(2),P(2)} = 10$ Hz, $^1J_{Pt(2),P(3)} = 2581$ Hz, $^1J_{Pt(2),P(4)} = 3794$ Hz, $^1J_{Pt(2),Pt(1)} = 1340$ Hz) ppm.

Reaction of 1 with para-H_2. For the PHIP experiments, hydrogen enriched in the para spin state was prepared by storing H_2 over Fe_2O_3 at 77 K for 3−4 h.[53]

^1H para-hydrogen spectra were performed on a JEOL EX-400 spectrometer operating at 399.65 MHz. All reactions with para-H_2 were carried out in a 5 mm NMR tube equipped with a J. Young valve. ALTADENA and PASADENA experiments were performed in order to detect hyperpolarized signals. In the ALTADENA experiment 6.8 bar of para-H_2 was added to frozen solutions of the metal complex (0.4 mL, 50 mM); the sample was warmed, shaken, and introduced into the magnet, where ^1H spectra were recorded by a single scan using a 45° pulse. In the PASADENA experiment the solution containing the sample under investigation (0.4 mL, 50 mM) was introduced into the magnet and the gas supplied through a capillary inserted into the NMR tube. NMR spectra (16 scans) were acquired 1−2 s after stopping the gas flow. rf pulses of 45° were used to maximize the hyperpolarized PASADENA signal.

Deuteration of 1. The deuterated compounds **2**-d_2 and **3**-d_2 were prepared in yields higher than 95% by following the procedures described above for the synthesis of their unlabeled analogues **2** and **3**, using dry D_2 in place of H_2.

Main NMR features of **2**-d_2 are as follows. ^2H NMR (CH_2Cl_2, 298 K): δ −1.4 (m, t-D, $^2J_{D,P(1)} = 18$ Hz, $^2J_{D,P(2)} = 4$ Hz, $^1J_{D,Pt(1)} = 150$ Hz), −4.2 (m, μ-D, $^2J_{D,P(2)} = 10$ Hz, $^2J_{D,P(4)} = 10$ Hz,$^1J_{D,Pt(1)} = 88$ Hz, $^1J_{D,Pt(2)} = 95$ Hz) ppm. $^{31}P\{^1H\}$ NMR (CH_2Cl_2, 298 K): δ 118.8 (d, P(1), $^2J_{P(1),P(3)} = 244$ Hz, $^1J_{P(1),P(t1)} = 1587$ Hz, $^1J_{P(1),Pt(2)} = 1090$ Hz), 73.5 (d, P(3), $^2J_{P(3),P(1)} = 244$ Hz, $^1J_{P(3),Pt(2)} = 2462$ Hz), 12.1 (br, P(4), $^3J_{P(4),P(2)} = 49$ Hz, $^2J_{P(4),P(3)} = 21$ Hz, $^1J_{P(4),Pt(2)} = 3930$), 9.6 (d, P(2), $^3J_{P(2),P(4)} = 47$ Hz, $^1J_{P(2),Pt(1)} = 3931$ Hz, $^2J_{P(2),Pt(2)} = 201$ Hz) ppm.

Main NMR features of **3**-d_2 are as follows. ^2H NMR (CH_2Cl_2, 298 K): δ −5.4 to −6.0 (t-D + μ-D) ppm. $^{31}P\{^1H\}$ NMR (CH_2Cl_2, 298 K): δ 132.8 (pseudo t, P(1), $^2J_{P(1),P(2)} = 256$ Hz, $^2J_{P(1),P(3)} = 260$ Hz, $^2J_{P(1),P(4)} = 16$ Hz, $^1J_{P(1),Pt(1)} = 2053$ Hz, $^1J_{P(1),Pt(2)} = 1206$ Hz), 80.4 (d, P(3), $^2J_{P(3),P(1)} = 260$ Hz, $^1J_{P(3),Pt(2)} = 2570$ Hz), 16.0 (d, P(2), $^2J_{P(2),P(1)} = 256$ Hz, $^1J_{P(2),Pt(1)} = 2560$ Hz, $^2J_{P(2),Pt(2)} = 10$ Hz), 11.3 (br, P(4), $^1J_{P(4),Pt(2)} = 3759$ Hz) ppm.

Dehydrogenation of 2. Solid **2** (20 mg) was put in a J-valve NMR tube, which was warmed at 323 K and put under high vacuum. After 3 h the system was cooled to room temperature, C_6D_6 was added, and $^{31}P\{^1H\}$ and ^1H NMR spectra were recorded, revealing the formation of **1** (ca. 80% based on ^{31}P) and a small amount (ca. 20%) of **3**.

Determination of the Kinetic Isotope Effect (KIE) for the Addition of H_2 to 1. In an NMR tube, deuterium gas was bubbled at room temperature (flow rate 0.2 mL/min) through a solution of 30.0 mg of **1** dissolved in 0.3 mL of CD_2Cl_2. During this time ^{31}P NMR spectra were recorded every 30 min for 6 h. Under identical conditions, dihydrogen was bubbled through a solution of **1** and the ^{31}P NMR spectra were periodically recorded. The KIE was determined to be the ratio of the reaction times for D_2/H_2 for the two reactions when the spectra appeared to be superimposable. By ^{31}P NMR (D_2 addition) and $^{31}P\{^1H\}$ NMR (H_2 addition) analyses, the complete consumption of **1** was evaluated to occur in 330 and 230 min, respectively. Thus, the D_2/H_2 isotope effect k_H/k_D was determined to be roughly 1.4.

Isotopic Exchange of 2 in the Solid State. Solid **2** (31 mg) was put in a J-valve NMR tube under 1 bar of D_2 and left under sonication at room temperature for 2 days. Then, D_2 was vented and to the solid was added 0.5 mL of toluene under dinitrogen. The resulting solution was used for ^2H NMR analysis, which revealed the formation of **3**-d_2. This can be explained either by isotopic exchange leading to **2**-d_2 followed by isomerization to **3**-d_2 or by isomerization to **3** followed by isotopic exchange. We have therefore put solid **3** under 1 bar of D_2 under the same conditions reported above, but no deuteration of the compound was observed. This demonstrates the occurrence of isotopic exchange for **2** also in the solid state.

Reactivity of 2 with $PHCy_2$. Compound **2** (60.0 mg, 0.050 mmol) was dissolved in 0.4 mL of C_6D_6, and $PHCy_2$ (0.040 mL, 0.20 mmol) was added, causing an immediate darkening of the solution. The $^{31}P\{^1H\}$ NMR recorded after 20 min of stirring revealed the presence of *cis*-[$(PHCy_2)_2$(H)Pt(μ-PCy_2)Pt($PHCy_2$)(H)(κP-P(O)Cy_2)](*Pt*−*Pt*) (**5**) and of free $PHCy_2$. The same complex is obtained when **3** is reacted with excess $PHCy_2$. Complex **5** was characterized in solution due to difficulties encountered in separating it from unreacted $PHCy_2$.

Spectroscopic Features of [$(PHCy_2)_2$(H)Pt(μ-PCy_2)Pt($PHCy_2$)(H){κP-P(O)Cy_2}] (5). ^1H NMR (C_6D_6, 298 K): δ −3.61 (m, H(1), $^2J_{H(1),P(1)} = 4$ Hz, $^2J_{H(1),P(2)} = 20$ Hz,$^2J_{H(1),P(3)} = 175$ Hz, $^1J_{H(1),Pt(1)} = 947$ Hz), 5.53 (m, H(2), $^1J_{H(2),P(2)} = 358$ Hz), 4.07 (m, H(3), $^1J_{H(3),P(3)} = 310$ Hz) −4.84 (m, H(4), $^2J_{H(4),P(1)} = 24$ Hz, $^2J_{H(4),P(4)} = 15$ Hz,$^2J_{H(4),P(5)} = 173$ Hz,$^1J_{H(4),Pt(2)} = 1004$ Hz), 3.76 (m, H(5), $^1J_{H(5),P(5)} = 290$ Hz) ppm. $^{31}P\{^1H\}$ NMR (C_6D_6, 298 K): δ 4.4 (dd, P(1), $^2J_{P(1),P(2)} = 226$ Hz, $^2J_{P(1),P(4)} = 307$ Hz, $^1J_{P(1),Pt(1)} = 2160$ Hz, $^1J_{P(1),Pt(2)} = 1402$ Hz), 12.6 (d, P(2), $^2J_{P(2),P(1)} = 226$ Hz, $^1J_{P(2),Pt(1)} = 2056$ Hz), 12.4 (br, P(3), $^1J_{P(3),Pt(1)} = 2026$ Hz), 90.2 (d, P(4), $^2J_{P(4),P(1)} = 307$ Hz, $^1J_{P(4),Pt(2)} = 2634$ Hz), 26.2 (s, P(5), $^1J_{P(5),Pt(2)} = 2052$ Hz) ppm. $^{195}Pt\{^1H\}$ NMR (C_6D_6, 298 K): δ −5148 (ddd, Pt(1), $^1J_{Pt(1),P(1)} = 2160$ Hz, $^1J_{Pt(1),P(2)} = 2056$ Hz, $^1J_{Pt(1),P(3)} = 2026$ Hz), −4908 (ddd, Pt(2), $^1J_{Pt(2),P(1)} = 1402$ Hz, $^1J_{Pt(2),P(4)} = 2634$ Hz, $^1J_{Pt(2),P(5)} = 2052$ Hz) ppm.

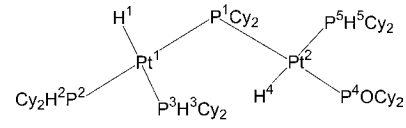

5

Acknowledgment. We thank the Italian MIUR (PRIN 2007, project prot. 2007X2RLL2) and COST Phosphorus Science Network (PhoSciNet, project CM0802) for financial support and Dr. A. Sibahoui and Prof. T. Repo (University of Helsinki, Helsinki, Finland) for HR-MS analyses.

Supporting Information Available: Figures and tables giving NMR spectra of compounds **2**, **2**-d_2, **3**, and **3**-d_2, the HR-MS spectrum of **3**, Cartesian coordinates of compounds, intermediates, and transition states, gas-phase and solution energies for the heterolytic and homolytic hydrogenation of **1** and for the intramolecular isomerization of **2**, hydrogen/deuterium kinetic isotopic effects, energy profile for the associative mechanism of the **2** → **3** isomerization, and optimized geometries of the intermediates **F**, **G**, **TS$_3$**, and **TS$_5$**. This material is available free of charge via the Internet at http://pubs.acs.org.

JA909747R

(53) Canet, D.; Aroulanda, C.; Mutzenhardt, P.; Aime, S.; Gobetto, R.; Reineri, F. *Concepts Magn. Reson., Part A* **2006**, *28A*, 321.